ICES REPORT 13-15

June 2013

A phase field approach to the fluid filled fracture surrounded by a poroelastic medium

by

Andro Mikelic, Mary F. Wheeler, Thomas Wick

The Institute for Computational Engineering and Sciences
The University of Texas at Austin
Austin, Texas 78712

Reference: Andro Mikelic, Mary F. Wheeler, Thomas Wick, A phase field approach to the fluid filled fracture surrounded by a poroelastic medium, ICES REPORT 13-15, The Institute for Computational Engineering and Sciences, The University of Texas at Austin, June 2013.

A phase field approach to the fluid filled fracture surrounded by a poroelastic medium*

Andro Mikelić †
Université de Lyon, CNRS UMR 5208,
Université Lyon 1, Institut Camille Jordan,
43, blvd. du 11 novembre 1918, 69622 Villeurbanne Cedex, France

Mary F. Wheeler, Thomas Wick
The Center for Subsurface Modeling,
Institute for Computational Engineering and Sciences
The University of Texas at Austin, 201 East 24th Street
Austin, TX 78712, U. S. A.

June 5, 2013

Abstract

In this paper we present an incremental formulation of the phase field model for a fluid filled crack in a poroelastic medium. The mathematical model represents a linear elasticity system with fading elastic moduli as the crack grows, that is coupled with an elliptic variational inequality for the phase field variable. The convex constraint of the variational inequality assures the irreversibility and entropy compatibility of the crack formation. We construct a finite dimensional approximation and demonstrate its solvability. Using compactness and monotonicity arguments we prove that solutions to the discretized problem converge to a solution of the incremental problem. We present a discretization technique

*A.M. would like to thank *Institute for Computational Engineering and Science (ICES)*, UT Austin for hospitality during his sabbatical stay from February to July, 2013. The research by M. F. Wheeler was partially supported by the U.S. Department of Energy, Office of Science, Office of Basic Energy Sciences through *DOE Energy Frontier Research Center: The Center for Frontiers of Subsurface Energy Security (CFSES)* under Contract No. DE-FG02-04ER25617, MOD. 005.

†E-mail: `Andro.Mikelic@univ-lyon1.fr`

applied to different scenarios in two and three dimensions. Computational results of benchmark problems are provided that demonstrate the effectiveness of this approach in treating fracture propagation.

Keywords Hydraulic fracturing, Phase field formulation, Nonlinear elliptic system, Computer simulations, Poroelasticity
AMS classcode 35B25;

1 Introduction

The coupling of flow and geomechanics in porous media is a major research topic in energy and environmental modeling. Of specific interest is induced hydraulic fracturing or hydrofracturing commonly known as fracking. This is technique used to release petroleum and natural gas that includes shale gas, tight gas, and coal seam gas for extraction. Here fracking creates fractures from a wellbore drilled into reservoir rock formations. In 2012, more than one million fracturing jobs were performed on oil and gas wells in the United States and this number continues to grow. Clearly there are economic benefits of extracting vast amounts of formerly inaccessible hydrocarbons. In addition, there are environmental benefits of producing natural gas, much of which is produced in the United States from fracking. Opponents to fracking point to environmental impacts such as contamination of ground water, risks to air quality, migration of fracturing chemical and surface contamination from spills to name a few. For these reason, hydraulic fracturing is being heavily scrutinized resulting in the need for accurate and robust mathematical and computational models for treating fluid field fractures surrounded by a poroelastic medium.

Even in the most basic formulation, hydraulic fracturing is complicated to model since it involves the coupling of (i) mechanical deformation; (ii) the flow of fluids within the fracture and in the reservoir; (iii) fracture propagation. Generally, rock deformation is modeled using the theory of linear elasticity which can be represented by an integral equation that determines a relationship between fracture width and the fluid pressure. Fluid flow in the fracture is modeled using lubrication theory that relates fluid flow velocity, fracture width and the gradient of pressure. Fluid flow in the reservoir is modeled as a Darcy flow and the respective fluids are coupled through a leakage term. The criterion for fracture propagation is usually given by the conventional energy-release rate approach of linear elastic fracture mechanics (LEFM) theory; that is the fracture propagates if the stress intensity factor at the tip matches the rock toughness. Detailed discussion of the development of hydraulic fracturing models for use in petroleum engineering can be found in [1] and in mechanical engineering and hydrology in [19], [7], [13] and in references therein.

Major difficulties in simulating hydraulic fracturing in a deformable porous medium are the coupling of a multi-phase reservoir simulator and in treating crack propagation. In [17] and [18] an iterative coupling algorithm was analyzed and computational results presented demonstrating the computational effectiveness of this method for modeling poroelastic systems without cracks by decoupling flow and geomechanics. In this paper we present an incremental formulation of a phase field model for a fluid filled crack surrounded by a poroelastic medium. The mathematical model involves the coupling of a linear elasticity system with an elliptic variational inequality for the phase field variable. With this approach, branching of fractures and heterogeneities in mechanical properties can be effectively treated as demonstrated numerically in Section 5. Moreover, iterative coupling can be applied in decoupling fluid and mechanics:

Iterative coupling is a sequential procedure where either the flow or the mechanics is solved first followed by solving the other problem using the latest solution information. At each time step the procedure is iterated until the solution converges within an acceptable tolerance. There are four well-known iterative coupling procedures and we are interested primarily in one called the **fixed stress split** iterative method.

In order to fix ideas we address the simplest model of real applied importance, namely, the quasi-static single phase Biot system. Let $\mathcal{C}$ denote any open set homeomorphic to an ellipsoid in $\mathbb{R}^3$ (a crack set). Its boundary is a closed surface $\partial\mathcal{C}$. The quasi-static Biot equations (see e.g. [22]) are an elliptic-parabolic system of PDEs, valid in the poroelastic domain $\Omega = (0,L)^3 \setminus \overline{\mathcal{C}}$, where for every $t \in (0,T)$ we have

$$\sigma^{por} - \sigma_0 = \mathcal{G}e(\mathbf{u}) - \alpha pI; \quad - \text{ div } \{\sigma^{por}\} = \rho_b \mathbf{g}; \tag{1}$$

$$\partial_t \big(\frac{1}{M} p + \text{ div } (\alpha \mathbf{u}) \big) + \text{ div } \{ \frac{\mathcal{K}}{\eta} (\rho_f \mathbf{g} - \nabla p) \} = f. \tag{2}$$

Boundary conditions for the general situation involve displacement and traction as well as pressure and flux, prescribed on portions of the boundary.
The important parameters and unknowns are given in the Table 1.

We make the following hypothesis on the effective coefficients

(H1) α, η , M and ρ_b are positive constants.

(H2) $\mathcal{K}$ is a symmetric uniformly positive definite matrix, with the smallest eigenvalue k and largest eigenvalue k^*. Furthermore, for any symmetric matrix B we have

$$\mathcal{G}B : B \geq a|B|^2 + K_{dr}(TrB)^2, \tag{3}$$

where K_{dr} is the drained bulk modulus.

SYMBOL	*QUANTITY*	*UNITY*
$\mathbf{u}$	displacement	m
p	fluid pressure	Pa
σ^{por}	total poroelasticity tensor	Pa
$e(\mathbf{u}) = (\nabla \mathbf{u} + \nabla^{\tau} \mathbf{u})/2$	linearized strain tensor	dimensionless
$\mathcal{K}$	permeability	Darcy
α	Biot's coefficient	dimensionless
ρ_b	bulk density	kg/m^3
η	fluid viscosity	kg/m sec
M	Biot's modulus	Pa
$\mathcal{G}$	Gassman rank-4 tensor	Pa

Table 1: *Unknowns and effective coefficients*

(H3) We have

$$\rho_b \mathbf{g} = - \text{ div } \sigma_0. \tag{4}$$

The *fixed stress split* iterative method consists in imposing constant volumetric mean total stress. This means that the $\sigma_v = \sigma_{v,0} + K_{dr} \text{ div } \mathbf{u} I - \alpha p I$ is kept constant at the half-time step. The iterative process reads as follows

$$\Big(\frac{1}{M} + \frac{\alpha^2}{K_{dr}} \Big) \partial_t p^{n+1} + \text{ div } \{ \frac{\mathcal{K}}{\eta} (\rho_f \mathbf{g} - \nabla p^{n+1}) \} =$$

$$- \frac{\alpha}{K_{dr}} \partial_t \sigma_v^n + f = f - \alpha \text{ div } \partial_t \mathbf{u}^n + \frac{\alpha^2}{K_{dr}} \partial_t p^n; \tag{5}$$

$$- \text{ div } \{ \mathcal{G} e(\mathbf{u}^{n+1}) \} + \alpha \nabla p^{n+1} = 0; \tag{6}$$

Remark 1. *We remark that the fixed stress approach is useful in employing existing reservoir simulators in that (5) can be extended to treat the mass balance equations arising in black oil or compositional flows and allows decoupling of multiphase flow and elasticity.*

Interest in the system (5)-(6) is based on its robust numerical convergence and on the following result

Theorem 1. *(see [17]) Let us suppose hypothesis (**H1**)-(**H3**) and initial and appropriate boundary conditions. Then the solution operator $\mathcal{S}$, mapping $\{\mathbf{u}^n, p^n\}$ to $\{\mathbf{u}^{n+1}, p^{n+1}\}$ is a contraction on $V_T \times W_T$, with*

$$V_T = \{ \mathbf{z} \in C([0,T]; H_0^1(\Omega)^3) \mid \partial_t e(\mathbf{z}) \in L^2((0,T) \times \Omega)^9 \} \tag{7}$$

$$W_T = \{ r \in H^1(\Omega \times (0,T)) \mid r \in C([0,T]; H^1(\Omega)) \}, \tag{8}$$

with contraction constant $\gamma_{FS} = \dfrac{M\alpha^2}{K_{dr} + M\alpha^2} < 1$. The corresponding unique fixed point satisfies equations (1)-(2).

With this strategy, we consider a realistic hydraulic fracture description in a poroelastic medium as a mathematical model of a fluid filled crack. Recently, numerical phase field experiments of a fluid filled quasi-static brittle fracture were undertaken by Bourdin et al. in [6]. Here our formulation follows Francfort and Marigo's variational approach to elastic fractures ([10] and [5]) and represents an extension to cracks in a poroelastic medium containing a viscous fluid.

Following Griffith's criterion, we suppose that the crack propagation occurs when the elastic energy restitution rate reaches its critical value G_c. If τ is the traction force applied at the part of the boundary $\partial_N\Omega$, then we associate to the crack $\mathcal{C}$ the following total energy

$$E(\mathbf{u}, \mathcal{C}) = \int_\Omega \frac{1}{2}\mathcal{G}e(\mathbf{u}) : e(\mathbf{u})\, dx - \int_{\partial_N\Omega} \tau\cdot\mathbf{u}\, dS - \int_\Omega \alpha p_B \text{div }\mathbf{u}\, dx + G_c\mathcal{H}^2(\mathcal{C}), \quad (9)$$

where p_B is the poroelastic medium pressure calculated in the previous iterative coupling step and $\alpha \in (0, 1)$ is the Biot coefficient.

This energy functional is then minimized with respect to the kinematically admissible displacements $\mathbf{u}$ and any crack set satisfying a crack growth condition. The computational modeling of this minimization problem should treat complex crack topologies and requires approximation of the crack location and of its length. This can be overcome by regularizing the sharp crack surface topology in the solid by diffusive crack zones described by a scalar auxiliary variable. This variable is a phase-field that interpolates between the unbroken and the broken states of the material. As previously stated above for the purely solid mechanics problem variational methods were introduced by Francfort and Marigo.

A related approach is diffusive crack modeling, developed by Miehe et al in [15] and based on the introduction of a crack phase-field. They propose a thermodynamically consistent framework for phase-field models of quasi-static crack propagation in elastic solids, together with incremental variational principles.

The outline of our paper is as follows: Based on the approach of Francfort and Marigo, we introduce a phase field model for a fluid filled crack in Section 2 and give an incremental formulation. Here we take into account the stress field coming from the crack and the pressure gradient, calculated by the previous fixed stress split model. In Section 3 we present a mathematical analysis of the incremental problem. In Section 4 the numerical method is briefly explained. Finally in Section 5 we provide numerical experiments for classical benchmark cases, e.g. Sneddon's pressurized crack with constant fluid pressure (see Subsection 5.2 and [20]).

2 Incremental phase field formulation

We introduce the time-dependent crack phase field φ, defined on $(0, L)^3 \times (0, T)$. The regularized crack functional reads

$$\Gamma_\varepsilon(\varphi) = \int_{(0,L)^3} (\frac{1}{2\varepsilon}(1-\varphi)^2 + \frac{\varepsilon}{2}|\nabla\varphi|^2)\ dx = \int_{(0,L)^3} \gamma(\varphi, \nabla\varphi)\ dx, \tag{10}$$

where γ is the crack surface density per unit volume. This regularization of $\mathcal{H}^2(\mathcal{C})$, in the sense of the $\Gamma-$limit when $\varepsilon \to 0$, was used in [4].

Our further considerations are based on the fact that evolution of cracks is fully dissipative in nature. First, the crack phase field φ is intuitively a regularization of $1 - \mathbb{1}_{\mathcal{C}}$ and we impose its negative evolution

$$\partial_t\varphi \leq 0. \tag{11}$$

Next we follow [15] and [6] and replace energy (9) by a global constitutive dissipation functional for a rate independent fracture process. that is

$$E_\varepsilon(\mathbf{u}, \varphi) = \int_{(0,L)^3} \frac{1}{2}\big((1-k)\varphi^2 + k\big)\mathcal{G}e(\mathbf{u}) : e(\mathbf{u})\ dx - \int_{\partial_N\Omega} \tau \cdot \mathbf{u}\ dS -$$
$$\int_{(0,L)^3} \alpha\varphi^{1+b} p_B \text{div}\ \mathbf{u}\ dx + G_c \int_{(0,L)^3} \left(\frac{1}{2\varepsilon}(1-\varphi)^2 + \frac{\varepsilon}{2}|\nabla\varphi|^2\right) dx,\ b \geq 0. \tag{12}$$

where b is a fixed nonnegative constant and k is a positive regularization parameter for elastic energy, with $k \ll \varepsilon$. The corresponding Euler-Lagrange equations read

$$\int_{(0,L)^3} \big((1-k)\varphi^2 + k\big)\mathcal{G}e(\mathbf{u}) : e(\mathbf{w})\ dx - \int_{\partial_N\Omega} \tau \cdot \mathbf{w}\ dS -$$
$$\int_{(0,L)^3} \alpha\varphi^{1+b} p_B\ \text{div}\ \mathbf{w}\ dx = 0, \quad \text{for all admissible} \quad \mathbf{w}; \tag{13}$$

$$\int_{(0,L)^3} (1-k)\varphi(\psi - \varphi)\mathcal{G}e(\mathbf{u}) : e(\mathbf{u})\ dx + G_c \int_{(0,L)^3} \big(- \frac{1}{\varepsilon}(1-\varphi)(\psi - \varphi) +$$
$$\varepsilon\nabla\varphi \cdot \nabla(\psi - \varphi)\big)\ dx -$$
$$\int_{(0,L)^3} (1+b)\alpha\varphi^b(\psi - \varphi)p_B\ \text{div}\ \mathbf{u}\ dx \geq 0, \quad \text{for all admissible}\ \psi, \tag{14}$$

where $\partial_t\psi \leq 0$. This two-field formulation can be compared with the Model I formulation given in [15] (see page 1289). The only difference is that (14) is a variational inequality and in [15] an equation is imposed through penalisation. The constraint $\partial_t\psi \leq 0$ can be imposed by penalization and (14) then becomes a variational equation.

Nevertheless, the crack is filled with a fluid and system (13)-(14) is incomplete. If we think of the crack as of a 3D thin domain with width much less than length, then the lubrication theory can be applied. At the leading order the stress in $\mathcal{C}$ is $-p_f I$ and at the crack boundary we have the continuity of the contact force

$$\sigma \mathbf{n} = (\mathcal{G}e(\mathbf{u}) - \alpha p_B I)\mathbf{n} = -p_f \mathbf{n} \tag{15}$$

Before introducing the phase field, we eliminate the traction crack surface integrals and obtain

$$\int_\Omega \alpha p_B \text{div } \mathbf{w} \; dx + \int_{\partial\mathcal{C}} \sigma \mathbf{n}\mathbf{w} \; dS = \int_\Omega \alpha p_B \text{div } \mathbf{w} \; dx - \int_{\partial\mathcal{C}} p_f w_n \; dS =$$
$$\int_\Omega \alpha p_B \text{div } \mathbf{w} \; dx - \int_\Omega \text{div } (p_B \mathbf{w}) \; dx + \int_{\partial_N\Omega} p_B w_n \; dS = \int_\Omega (\alpha - 1) p_B \text{div } \mathbf{w} \; dx -$$
$$\int_\Omega \nabla p_B \mathbf{w} \; dx + \int_{\partial_N\Omega} p_B w_n \; dS.$$

Remark 2. *Setting $\alpha = 1$, $p = p_f$ in the crack and $p = p_B$ in the poroelastic medium, then the above calculations yield*

$$\int_\Omega \alpha p_B \, div \, \mathbf{w} \; dx - \int_{\partial\mathcal{C}} p_f w_{n,poroelastic} \; dS = \int_{(0,L)^3} \alpha p \, div \, \mathbf{w} \; dx +$$
$$\int_{\mathcal{C}} \nabla p \mathbf{w} \; dx - \int_{\mathcal{C}} div \; (p\mathbf{w}) \; dx - \int_{\partial\mathcal{C}} p_f w_{n,poroelastic} \; dS =$$
$$\int_{(0,L)^3} \alpha p \, div \, \mathbf{w} \; dx + \int_{\mathcal{C}} \nabla p \mathbf{w} \; dx - \int_{\partial\mathcal{C}} p (w_{n,poroelastic} - w_{n,crack}) \; dS.$$

The last term coincides with the virtual work of the pressure force as introduced in [8] and applied in [6].

Next we have

$$-\int_{\partial_N\Omega} \tau \cdot \mathbf{w} \; dS + \int_{\partial\mathcal{C}} p w_n \; dS - \int_\Omega \alpha p \text{ div } \mathbf{w} \; dx = -\int_\Omega (\alpha - 1) p \text{ div } \mathbf{w} \; dx +$$
$$\int_\Omega \nabla p \mathbf{w} \; dx - \int_\Omega \text{div } (\mathcal{T}\mathbf{w}) \; dx = -\int_\Omega (\alpha - 1) p \text{ div } \mathbf{w} \; dx +$$
$$\int_\Omega (\nabla p - \text{ div } \mathcal{T}) \mathbf{w} \; dx - \int_\Omega \mathcal{T} : e(\mathbf{w}) \; dx, \tag{16}$$

where $\mathcal{T}$ is a smooth symmetric 3×3 matrix with compact support in a neighborhood of $\partial(0, L)^3$, such that $\mathcal{T}\mathbf{n} = \tau + p\mathbf{n}$ on $\partial_N(0, L)^3$. We note that $\mathcal{T}$ is chosen to avoid interaction between the crack $\mathcal{C}$ and $\partial_N\Omega$.

After the above transformations, we have the following phase field formulation of equation (13)

$$\int_{(0,L)^3} \big((1-k)\varphi^2 + k\big)\mathcal{G} e(\mathbf{u}) : e(\mathbf{w})\ dx - \int_{(0,L)^3} (\alpha-1)\varphi^{1+b} p \ \mathrm{div}\ \mathbf{w}\ dx +$$
$$\int_{(0,L)^3} \varphi^{1+b}(\nabla p - \ \mathrm{div}\ \mathcal{T})\mathbf{w}\ dx - \int_{(0,L)^3} \varphi^{1+b}\mathcal{T} : e(\mathbf{w})\ dx = 0,$$
$$\text{for all admissible } \mathbf{w}. \tag{17}$$

We are working with the quasi-static formulation and velocity changes are small. Hence, we are able to replace our time derivative in inequality (11) with a discretized one, namely we work with an incremental formulation

$$\partial_t \varphi \to \partial_{\Delta t}\varphi = (\varphi - \varphi_p)/(\Delta t),$$

where $\Delta t > 0$ is the time step and φ_p is the phase field from the previous time step. After time discretization, our quasistatic equations (14), (17) change to a stationary problem, called the incremental problem.

In the classical case of elastic cracks one has $0 \le \varphi \le 1$. We will establish this property for the continuous in space incremental problem. Nevertheless, for the incremental problem discretized in spaces and penalized to satisfy the obstacle condition $\varphi \le \varphi_p$, the phase field unknown φ may be negative and take values larger than 1. Thus, for the discretized equations we use φ_+ instead of φ in terms where negative φ could lead to a wrong conclusion and make cut-offs where φ could be larger than 1.

Let us set

$$\mathcal{F} = -(\alpha-1)pI - \mathcal{T}, \qquad \mathbf{f} = \nabla p - \ \mathrm{div}\ \mathcal{T}. \tag{18}$$

To avoid that high gradients in the neighborhood of a crack lead also to non-physical large displacements, we add a friction term $\beta\partial_t\mathbf{u}$, $\beta > 0$.
We assume on the part of the boundary $\partial_D(0,L)^3$ the homogeneous Dirichlet conditions for the displacement and choose as functional space of admissible displacements $V_U = \{\mathbf{z} \in H^1((0,L)^3)^3 \mid \mathbf{z} = 0 \ \text{on}\ \ \partial_D(0,L)^3\ \}$. Equation (17) becomes

$$\int_{(0,L)^3} \big((1-k)\varphi^2 + k\big)\mathcal{G} e(\mathbf{u}) : e(\mathbf{w})\ dx + \int_{(0,L)^3} \beta\varphi\partial_{\Delta t}\mathbf{u}\cdot\mathbf{w}\ dx +$$
$$\int_{(0,L)^3} \varphi^{1+b}(\mathcal{F} : e(\mathbf{w}) + \mathbf{f}\cdot\mathbf{w})\ dx = 0,\ \forall \mathbf{w} \in V_U, \tag{19}$$

or in the differential form

$$\beta\varphi\partial_{\Delta t}\mathbf{u} - \text{ div }\Big(\big((1-k)\varphi^2+k\big)\mathcal{G}e(\mathbf{u})\Big) + \varphi^{1+b}\mathbf{f} - \\ \text{div }(\varphi^{1+b}\mathcal{F}) = 0 \quad \text{in} \quad (0,L)^3, \tag{20}$$

$$\mathbf{u} = 0 \quad \text{on} \quad \partial_D(0,L)^3, \tag{21}$$

$$\big((1-k)\varphi^2+k\big)\mathcal{G}e(\mathbf{u})\mathbf{n} = -\varphi^{1+b}\mathcal{F}\mathbf{n} \quad \text{on} \quad \partial_N(0,L)^3. \tag{22}$$

For $\alpha = 0$ and $\beta = 0$ we recover the pressure term from [6] and [8].
It remains to write the phase field equation. In the differential form it reads

$$\partial_{\Delta t}\varphi \le 0 \quad \text{on} \quad (0,L)^3 \quad \text{and} \quad \frac{\partial\varphi}{\partial\mathbf{n}} = 0 \quad \text{on} \quad \partial(0,L)^3; \tag{23}$$

$$-G_c\varepsilon\Delta\varphi - \frac{G_c}{\varepsilon}(1-\varphi) + (1-k)\mathcal{G}e(\mathbf{u}) : e(\mathbf{u})\varphi + \\ (1+b)\varphi^b(\mathcal{F} : e(\mathbf{u}) + \mathbf{f}\cdot\mathbf{u}) \le 0 \quad \text{in} \quad (0,L)^3, \tag{24}$$

$$\Big\{ - G_c\varepsilon\Delta\varphi - \frac{G_c}{\varepsilon}(1-\varphi) + (1-k)\mathcal{G}e(\mathbf{u}) : e(\mathbf{u})\varphi + \\ (1+b)\varphi^b(\mathcal{F} : e(\mathbf{u}) + \mathbf{f}\cdot\mathbf{u})\Big\}\partial_{\Delta t}\varphi = 0 \text{ in } (0,L)^3. \tag{25}$$

Note that for $b = 0$, φ^b reads $H(\varphi)$, where H is Heaviside's function, $H(0) = 0$ and $H(t) = 1$ for $t > 0$.

In order to write the variational form, we introduce the convex set K by

$$K = \{\psi \in H^1((0,L)^3) \mid \psi \le \varphi_p \le 1 \text{ a.e. on } (0,L)^3\}. \tag{26}$$

The variational formulation is

$$\int_{(0,L)^3} (1-k)\varphi(\psi-\varphi)\mathcal{G}e(\mathbf{u}) : e(\mathbf{u})\, dx + G_c\int_{(0,L)^3}\big(-\frac{1}{\varepsilon}(1-\varphi)(\psi-\varphi) + \\ \varepsilon\nabla\varphi\cdot\nabla(\psi-\varphi)\big)\, dx + \int_{(0,L)^3}(1+b)\varphi^b(\mathcal{F} : e(\mathbf{u}) + \mathbf{f}\cdot\mathbf{u})\,(\psi-\varphi)\, dx \ge 0, \\ \forall\, \psi \in K\cap L^\infty((0,L)^3). \tag{27}$$

3 Well-posedness of the model

We will search for a solution to variational equation (19)-(27). A natural way would be to use the *Schauder-Tychonoff fixed point theorem*. Unfortunately the first term in equation (27) is not continuous with respect to weak convergence in H^1 and our strategy is different. We will prove that there is a solution for a finite dimensional approximation of equations (19)-(27) and then pass to the limit. Our goal is to prove

Theorem 2. *(Existence of a weak solution to the incremental phase field problem) Let $b, k > 0$ and $\mathcal{F}$, $\mathbf{f} \in W^{1,\infty}$, $\varphi_p \in H^1$, $0 \le \varphi_p \le 1$ a.e. on $(0,L)^3$. Then there exists $\{\mathbf{u}, \varphi\} \in V_U \times K$, $\varphi \ge 0$ a.e. on $(0,L)^3$, satisfying variational equations (19) and (27) and a priori estimates*

$$\frac{\beta}{2\Delta t}\int_{(0,L)^3} \varphi|\mathbf{u}|^2 \, dx + ||\sqrt{\varphi}\mathbf{u}||^2_{L^2} + ||\varphi e(\mathbf{u})||^2_{L^2} \le c; \tag{28}$$

$$G_c \int_{(0,L)^3} \Big(\frac{(\varphi - \varphi_p)^2}{\varepsilon} + \frac{(\varphi_p - 1)(\varphi - \varphi_p)}{\varepsilon} + \varepsilon |\nabla(\varphi - \varphi_p)|^2 \Big) \, dx + \\ ||\sqrt{\varphi} e(\mathbf{u})||^2_{L^2} + \sqrt{k} ||e(\mathbf{u})||^2_{L^2} \le \frac{c}{\sqrt{k}}. \tag{29}$$

3.1 A finite dimensional approximation

Let $\{\psi_r\}_{r\in\mathbb{N}}$ be a smooth basis for $H^1((0,L)^3)$ and $\{\mathbf{w}^r\}_{r\in\mathbb{N}}$ be a smooth basis for V_U. We start by defining a finite dimensional approximation problem:

Definition 1. *Let $\delta > 0$ and $M \in \mathbb{N}$. Let $\tilde{\varphi} = \inf\{1, \varphi_+\}$. The pair $\{\mathbf{u}^M, \varphi^M\}$, $\mathbf{u}^M = \sum_{r=1}^M a_r \mathbf{w}^r$ and $\varphi^M = \sum_{r=1}^M b_r \psi_r$, is a finite dimensional penalized approximative solution for problem (19) and (27) if it satisfies*

$$\int_{(0,L)^3} \big((1-k)(\tilde{\varphi}^M)^2 + k\big) \mathcal{G} e(\mathbf{u}^M) : e(\mathbf{w}^r) \, dx + \int_{(0,L)^3} \beta \varphi^M_+ \partial_{\Delta t} \mathbf{u}^M \cdot \mathbf{w}^r \, dx \\ + \int_{(0,L)^3} (\tilde{\varphi}^M)^{b+1} (\mathcal{F} : e(\mathbf{w}^r) + \mathbf{f} \cdot \mathbf{w}^r) \, dx = 0, \quad \forall r = 1, \dots, M, \tag{30}$$

$$G_c \int_{(0,L)^3} \big(-\frac{1}{\varepsilon}(1 - \varphi^M)\psi_r + \varepsilon \nabla\varphi^M \cdot \nabla\psi_r \big) \, dx + \int_{(0,L)^3} \frac{1}{\delta} (\partial_{\Delta t} \varphi^M)_+ \psi_r \, dx + \\ (1+b) \int_{(0,L)^3} (\tilde{\varphi}^M)^b (\mathcal{F} : e(\mathbf{u}^M) + \mathbf{f} \cdot \mathbf{u}^M) \psi_r \, dx + \\ \int_{(0,L)^3} (1-k) \tilde{\varphi}^M \psi_r \mathcal{G} e(\mathbf{u}^M) : e(\mathbf{u}^M) \, dx = 0, \quad \forall \, r = 1, \dots, M. \tag{31}$$

We note that in the elasticity equation (30) a friction term is added and in the phase field equation (31) a penalization term is used.

Proposition 1. *We suppose the hypotheses of Theorem 2. Then there exists a finite dimensional penalized approximative solution for problem (30)-(31) that satisfies the a priori estimate*

$$G_c \int_{(0,L)^3} \frac{(\varphi^M)^2}{\varepsilon} \, dx + \int_{(0,L)^3} \frac{1}{\Delta t \delta} (\varphi^M - \varphi_p)^2_+ \, dx + \frac{\beta}{\Delta t} \int_{(0,L)^3} \varphi^M_+ |\mathbf{u}^M|^2 \, dx + \\ k ||e(\mathbf{u}^M)||^2_{L^2} + ||\tilde{\varphi}^M e(\mathbf{u}^M)||^2_{L^2} \le \frac{c}{\varepsilon}, \tag{32}$$

where c is independent of M, k and ε.

Proof. Let $\xi = \{a_r, b_r\}_{r=1,\dots,M} = \{\xi_1, \xi_2\}$ and X the finite dimensional space spanned by the set of all such ξ. X is isomorphic to $\mathbb{R}^{2M}$ and we take the natural scalar product. After setting

$$
\begin{aligned}
P_{1,r}(\xi) = &\int_{(0,L)^3} \big((1-k)(\tilde{\varphi}^M)^2 + k\big)\mathcal{G}e(\mathbf{u}^M) : e(\mathbf{w}^r)\, dx + \int_{(0,L)^3} \beta\varphi_+^M \partial_{\Delta t}\mathbf{u}^M \cdot \mathbf{w}^r\, dx \\
&+ \int_{(0,L)^3} (\tilde{\varphi}^M)^{b+1}(\mathcal{F} : e(\mathbf{w^r}) + \mathbf{f}\cdot\mathbf{w}^r)\, dx, \quad r = 1,\dots,M; \qquad (33)
\end{aligned}
$$

$$
\begin{aligned}
P_{2,r}(\xi) = &\int_{(0,L)^3} (1-k)\tilde{\varphi}^M\psi_r\mathcal{G}e(\mathbf{u}^M) : e(\mathbf{u}^M)\, dx + \int_{(0,L)^3} \frac{1}{\delta}(\partial_{\Delta t}\varphi^M)_+\psi_r\, dx + \\
&G_c\int_{(0,L)^3} \big(-\frac{1}{\varepsilon}(1-\varphi^M)\psi_r + \varepsilon\nabla\varphi^M\cdot\nabla\psi_r\big)\, dx + \\
&(1+b)\int_{(0,L)^3} (\tilde{\varphi}^M)^b(\mathbf{f}\cdot\mathbf{u}^M + \mathcal{F} : e(\mathbf{u}^M))\psi_r\, dx, \quad r = 1,\dots,M, \qquad (34)
\end{aligned}
$$

we see that problem (30)-(31) has a solution if and only if equation $P(\xi) = 0$ has a solution.

The nonlinear mapping P is obviously continuous between X and X. Using a well-known corollary[1] of Brouwer's fixed point theorem, it is enough to prove that $(P(\xi), \xi)_X > 0$ for ξ with sufficiently large norm. Existence of at least one root would follow.

We start by multiplying $P_{1,r}(\xi)$ by a_r and taking the sum with respect to r. It yields

$$
\begin{aligned}
(P_1(\xi), \xi_1) = &\int_{(0,L)^3} \big((1-k)(\tilde{\varphi}^M)^2 + k\big)\mathcal{G}e(\mathbf{u}^M) : e(\mathbf{u}^M)\, dx + \\
&\int_{(0,L)^3} \beta\varphi_+^M\partial_{\Delta t}\mathbf{u}^M\cdot\mathbf{u}^M\, dx + \int_{(0,L)^3} (\tilde{\varphi}^M)^{b+1}(\mathcal{F} : e(\mathbf{u}^M) + \mathbf{f}\cdot\mathbf{u}^M)\, dx. \qquad (35)
\end{aligned}
$$

We estimate terms one by one:

$$
\begin{aligned}
&\int_{(0,L)^3} \varphi_+^M\beta\partial_{\Delta t}\mathbf{u}^M\cdot\mathbf{u}^M\, dx \geq \frac{\beta}{2}\int_{(0,L)^3} \varphi_+^M\partial_{\Delta t}|\mathbf{u}^M|^2\, dx = \\
&\frac{\beta}{2}\int_{(0,L)^3} \partial_{\Delta t}(\varphi_+^M|\mathbf{u}^M|^2)\, dx - \frac{\beta}{2}\int_{(0,L)^3} |\mathbf{u}_p|^2\partial_{\Delta t}\varphi_+^M\, dx, \qquad (36)
\end{aligned}
$$

[1]Lemma 1.4. (see e.g. R. Temam, Navier-Stokes Equations, page 164) Let X be a finite dimensional Hilbert space with scalar product $(\cdot,\cdot)_X$ and norm $||\cdot||_X$ and let P be a continuous from X into itself such that

$$(P(\xi), \xi)_X > 0 \quad \text{for} \quad ||\xi||_X = R > 0.$$

Then there exists $\xi \in X$, $||\xi||_X \leq R$, such that $P(\xi) = 0$.

$$| \int_{(0,L)^3} (\tilde{\varphi}^M)^{b+1} \mathbf{f} \cdot \mathbf{u}^M \ dx| \leq ||\sqrt{\varphi_+^M} \mathbf{u}^M||_{L^2} \ ||\mathbf{f}||_{L^2}, \tag{37}$$

$$| \int_{(0,L)^3} (\tilde{\varphi}^M)^{b+1} \mathcal{F} : e(\mathbf{u}^M) \ dx| \leq ||\tilde{\varphi}^M e(\mathbf{u}^M)||_{L^2} \ ||\mathcal{F}||_{L^2}, . \tag{38}$$

The elastic energy terms yields

$$\int_{(0,L)^3} \big((1-k)(\tilde{\varphi}^M)^2 + k\big) \mathcal{G} e(\mathbf{u}^M) : e(\mathbf{u}^M) \ dx \geq$$
$$c_1 k ||e(\mathbf{u}^M)||_{L^2}^2 + c_3 ||\tilde{\varphi}^M e(\mathbf{u}^M)||_{L^2}^2. \tag{39}$$

After inserting (36)-(39) into (35), we get

$$(P_1(\xi), \xi_1) \geq \frac{\beta}{2} \int_{(0,L)^3} \partial_{\Delta t} (\varphi_+^M |\mathbf{u}^M|^2) \ dx + c_1 k ||e(\mathbf{u}^M)||_{L^2}^2 - c_5 - c_2 ||\sqrt{\varphi_+^M} \mathbf{u}^M||_{L^2}$$
$$+ \frac{c_3}{2} ||\tilde{\varphi}^M e(\mathbf{u}^M)||_{L^2}^2 - \frac{\beta}{2} \int_{(0,L)^3} |\mathbf{u}_p|^2 \partial_{\Delta t} \varphi_+^M \ dx. \tag{40}$$

Next we have

$$(P_2(\xi), \xi_2) = \int_{(0,L)^3} (1-k) \tilde{\varphi}^M \varphi_+^M \mathcal{G} e(\mathbf{u}^M) : e(\mathbf{u}^M) \ dx +$$
$$G_c \int_{(0,L)^3} \big(-\frac{1}{\varepsilon} (1-\varphi^M) \varphi^M + \varepsilon |\nabla \varphi^M|^2 \big) \ dx + \int_{(0,L)^3} \frac{1}{\delta} (\partial_{\Delta t} \varphi^M)_+ \varphi^M \ dx +$$
$$(1+b) \int_{(0,L)^3} (\mathcal{F} : e(\mathbf{u}^M) + \mathbf{f} \cdot \mathbf{u}^M) (\tilde{\varphi}^M)^b \varphi_+^M \ dx. \tag{41}$$

Estimating different terms is straightforward:

$$G_c \int_{(0,L)^3} -\frac{1}{\varepsilon} (1-\varphi^M) \varphi^M \ dx \geq -\frac{G_c L^3}{2\varepsilon} + G_c \int_{(0,L)^3} \frac{(\varphi^M)^2}{2\varepsilon} \ dx. \tag{42}$$

Next we note that

$$(\min\{x_+, 1\})^b x_+ \leq \min\{x_+, 1\} (1 + x_+)$$

which gives

$$| \int_{(0,L)^3} \mathcal{F} : e(\mathbf{u}^M) (\tilde{\varphi}^M)^b \varphi_+^M \ dx| \leq c_7 ||\tilde{\varphi}^M e(\mathbf{u}^M)||_{L^2} (1 + ||\varphi^M||_{L^2});$$
$$| \int_{(0,L)^3} \mathbf{f} \cdot \mathbf{u}^M (\tilde{\varphi}^M)^b \varphi_+^M \ dx| \leq c_8 ||\sqrt{\varphi_+^M} \mathbf{u}^M||_{L^2} ||\varphi^M||_{L^1};$$
$$| \int_{(0,L)^3} \frac{1}{\delta} (\partial_{\Delta t} \varphi^M)_+ \varphi^M \ dx| \geq \int_{(0,L)^3} \frac{1}{\delta \Delta t} (\varphi^M - \varphi_p)_+^2 \ dx.$$

Therefore, we have

$$(P_2(\xi), \xi_2) \geq G_c \int_{(0,L)^3} \big(\frac{(\varphi^M)^2}{2\varepsilon} + \varepsilon |\nabla \varphi^M|^2\big) \ dx + \int_{(0,L)^3} \frac{1}{\Delta t \delta} (\varphi^M - \varphi_p)_+^2 \ dx - \\ c_7 \big(||\sqrt{\varphi_+^M} \mathbf{u}^M||_{L^2} + ||\tilde{\varphi}^M e(\mathbf{u}^M)||_{L^2}\big)(1 + ||\varphi^M||_{L^2}) - \frac{G_c L^3}{2\varepsilon}. \qquad (43)$$

Next we have

$$|\frac{\beta}{2} \int_{(0,L)^3} |\mathbf{u}_p|^2 (\partial_{\Delta t} \varphi_+^M)_+ \ dx| \leq \int_{(0,L)^3} \frac{1}{4\Delta t \delta} (\varphi^M - \varphi_p)_+^2 \ dx + \frac{\beta^2 \delta}{4 \Delta t} \int_{(0,L)^3} |\mathbf{u}_p|^4 \ dx. \qquad (44)$$

Putting together (40) and (43), and using (44), yields

$$(P(\xi), \xi) = (P_1(\xi), \xi_1) + (P_2(\xi), \xi_2) \geq G_c \int_{(0,L)^3} \big(\frac{(\varphi^M)^2}{4\varepsilon} + \varepsilon |\nabla \varphi^M|^2\big) \ dx + \\ \int_{(0,L)^3} \frac{1}{4\Delta t \delta} (\varphi^M - \varphi_p)_+^2 \ dx + \frac{\beta}{2\Delta t} \int_{(0,L)^3} \varphi_+^M |\mathbf{u}^M|^2 \ dx + c_1 k ||e(\mathbf{u}^M)||_{L^2}^2 + \\ \tilde{c}_3 ||\tilde{\varphi}^M e(\mathbf{u}^M)||_{L^2}^2 - \frac{\tilde{c}_9}{\varepsilon}. \qquad (45)$$

It follows from (45) that $(P(\xi), \xi) > 0$ for $||\xi|| = R$, with sufficiently large R.

Obviously corresponding solutions $\{\mathbf{u}^M, \varphi^M\}$ satisfy a priori estimate (32).

□

Theorem 3. *Assume the hypotheses of Theorem 2. Then there exists* $\{\mathbf{u}^\delta, \varphi^\delta\} \in V_U \times H^1((0,L)^3)$ *satisfying the variational equations*

$$\int_{(0,L)^3} \big((1-k)(\tilde{\varphi}^\delta)^2 + k\big) \mathcal{G} e(\mathbf{u}^\delta) : e(\mathbf{w}) \ dx + \int_{(0,L)^3} \beta \varphi_+^\delta \partial_{\Delta t} \mathbf{u}^\delta \cdot \mathbf{w} \ dx + \\ \int_{(0,L)^3} (\tilde{\varphi}^\delta)^{b+1} (\mathcal{F} : e(\mathbf{w}) + \mathbf{f} \cdot \mathbf{w}) \ dx = 0, \quad \forall \ \mathbf{w} \in V_U, \qquad (46)$$

$$\int_{(0,L)^3} (1-k) \tilde{\varphi}^\delta \psi \mathcal{G} e(\mathbf{u}^\delta) : e(\mathbf{u}^\delta) \ dx + \\ G_c \int_{(0,L)^3} \big(-\frac{1}{\varepsilon}(1 - \varphi^\delta)\psi + \varepsilon \nabla \varphi^\delta \cdot \nabla \psi\big) \ dx + \int_{(0,L)^3} \frac{1}{\delta} (\partial_{\Delta t} \varphi^\delta)_+ \psi \ dx + \\ (1+b) \int_{(0,L)^3} (\tilde{\varphi}^\delta)^b (\mathbf{f} \cdot \mathbf{u}^\delta + \mathcal{F} : e(\mathbf{u}^\delta)) \psi \ dx = 0, \\ \forall \ \psi \in H^1((0,L)^3) \cap L^\infty((0,L)^3). \qquad (47)$$

and a priori estimate (32).

Proof. By Proposition 1 there is a solution $\{\mathbf{u}^M, \varphi^M\}$ for equations (30)-(31) satisfying a priori estimate (32). Therefore there exists $\{\mathbf{u}^\delta, \varphi^\delta\}$ and a subsequence, denoted by the same superscript, such that

$$\{\mathbf{u}^M, \varphi^M\} \to \{\mathbf{u}^\delta, \varphi^\delta\} \quad \text{weakly in } V_U \times H^1((0,L)^3),$$
$$\text{strongly in } \; L^q((0,L)^3)^4, \; q < 6, \quad \text{and a.e. on} \quad (0,L)^3, \; \text{ as } \; M \to \infty. \tag{48}$$

Passing to the limit in equation (30) is straightforward and we conclude that $\{\mathbf{u}^\delta, \varphi^\delta\}$ satisfies equation (46).

For passing to the limit in equation (31) we need strong convergence of $\{\mathbf{u}^M\}$ in V_U. We choose $\mathbf{w} = \mathbf{u}^M$ as test function in (46) and pass to the limit $M \to \infty$. It yields

$$\int_{(0,L)^3} \big((1-k)(\tilde\varphi^\delta)^2 + k\big)\mathcal{G}e(\mathbf{u}^\delta) : e(\mathbf{u}^\delta)\; dx + \int_{(0,L)^3} \beta\varphi_+^\delta \partial_{\Delta t}\mathbf{u}^\delta \cdot \mathbf{u}^\delta \; dx$$
$$+ \int_{(0,L)^3} (\tilde\varphi^\delta)^{b+1}(\mathcal{F} : e(\mathbf{u}^\delta) + \mathbf{f}\cdot\mathbf{u}^\delta)\; dx = 0. \tag{49}$$

Therefore we have the convergence of the weighted elastic energies

$$\lim_{M\to\infty} \int_{(0,L)^3} \big((1-k)(\tilde\varphi^M)^2 + k\big)\mathcal{G}e(\mathbf{u}^M) : e(\mathbf{u}^M)\; dx =$$
$$\int_{(0,L)^3} \big((1-k)(\tilde\varphi^\delta)^2 + k\big)\mathcal{G}e(\mathbf{u}^\delta) : e(\mathbf{u}^\delta)\; dx. \tag{50}$$

Using Fatou's lemma we have

$$\int_{(0,L)^3} \liminf_{M\to\infty} \big((1-k)(\tilde\varphi^M)^2 + k\big)\mathcal{G}e(\mathbf{u}^M) : e(\mathbf{u}^M)\; dx$$
$$\le \liminf_{M\to\infty} \int_{(0,L)^3} \big((1-k)(\tilde\varphi^M)^2 + k\big)\mathcal{G}e(\mathbf{u}^M) : e(\mathbf{u}^M)\; dx$$
$$= \int_{(0,L)^3} \big((1-k)(\tilde\varphi^\delta)^2 + k\big)\mathcal{G}e(\mathbf{u}^\delta) : e(\mathbf{u}^\delta)\; dx. \tag{51}$$

Consequently

$$\mathbf{u}^M \to \mathbf{u}^\delta \quad \text{strongly in} \quad V_U, \quad \text{as } \; M \to \infty. \tag{52}$$

For every $\psi \in L^\infty((0,L)^3) \cap H^1((0,L)^3)$, (52) implies

$$\lim_{M\to\infty} |\int_{(0,L)^3} \tilde\varphi^M \psi \mathcal{G}e(\mathbf{u}^M - \mathbf{u}^\delta) : e(\mathbf{u}^M - \mathbf{u}^\delta)\; dx| \to 0, \quad \text{as } \; M \to \infty,$$

and

$$\int_{(0,L)^3} \tilde{\varphi}^M \psi \mathcal{G} e(\mathbf{u}^M) : e(\mathbf{u}^M)\ dx = \int_{(0,L)^3} \tilde{\varphi}^M \psi \mathcal{G} e(\mathbf{u}^M - \mathbf{u}^\delta) : e(\mathbf{u}^M - \mathbf{u}^\delta)\ dx + 2\int_{(0,L)^3} \tilde{\varphi}^M \psi \mathcal{G} e(\mathbf{u}^M) : e(\mathbf{u}^\delta)\ dx - \int_{(0,L)^3} \tilde{\varphi}^M \psi \mathcal{G} e(\mathbf{u}^\delta) : e(\mathbf{u}^\delta)\ dx \to \int_{(0,L)^3} \tilde{\varphi}^\delta \psi \mathcal{G} e(\mathbf{u}^\delta) : e(\mathbf{u}^\delta)\ dx, \quad \text{as} \ \ M \to \infty. \tag{53}$$

Passing to the limit in equation (31) is now straightforward. We note that convergence (53) allows to establish strong convergence of $\{\varphi^M\}$ in $H^1((0,L)^3)$. $\square$

Corollary 1. *Assume the hypotheses of Theorem 2. Then φ^δ is nonnegative a.e. on $(0,L)^3$.*

Proof. If $\varphi_p \geq 0$ a.e., then $(\varphi^\delta_+ - \varphi_p)_+ \varphi^\delta_- = 0$. We take φ^δ_- as a test function in (47). It yields

$$0 \geq G_c \int_{(0,L)^3} \big(\varepsilon |\nabla \varphi^\delta_-|^2 - \frac{\varphi^\delta_-}{\varepsilon} + \frac{|\varphi^\delta_-|^2}{\varepsilon}\big)\ dx$$

and we see that φ^δ is nonnegative. $\square$

We remark that Corollary 1 fails for $b = 0$.

Our next step is to pass to the limit $\delta \to 0$.

3.2 Proof of Theorem 2

Proof. (of Theorem 2) We start by testing equation (46) by $\mathbf{w} = \mathbf{u}^\delta$. After repeating calculations described in the proof of Proposition 1, we arrive at an analogue of estimate (40)

$$\frac{\beta}{4\Delta t} \int_{(0,L)^3} \varphi^\delta |\mathbf{u}^\delta|^2\ dx + k||e(\mathbf{u}^\delta)||^2_{L^2} + ||\inf\{\varphi^\delta, 1\} e(\mathbf{u}^\delta)||^2_{L^2} \leq C + \frac{C\beta}{2} \int_{(0,L)^3} |\mathbf{u}_p|^2 (\partial_{\Delta t} \varphi^\delta)_+\ dx. \tag{54}$$

Next we test equation (47) with $\psi = \varphi^\delta$. After repeating calculations from the proof of Proposition 1, we arrive at an analogue of estimate (43)

$$G_c \int_{(0,L)^3} \big(\frac{(\varphi^\delta)^2}{2\varepsilon} + \varepsilon |\nabla \varphi^\delta|^2\big)\ dx + \int_{(0,L)^3} \frac{1}{2\Delta t \delta} (\varphi^\delta - \varphi_p)_+ \varphi^\delta\ dx \leq C\big(||\sqrt{\varphi^\delta} \mathbf{u}^\delta||_{L^2} + ||\inf\{\varphi^\delta, 1\} e(\mathbf{u}^\delta)||_{L^2}\big)(1 + ||\varphi^\delta||_{L^2}) + \frac{c_9}{\varepsilon}. \tag{55}$$

In order to get an estimate independent of δ, our strategy is to combine estimate (54) and estimate (55) multiplied by ε. Then the penalization term is used to control the right hand side of estimate (54), i. e. we need to bound the following combination

$$\int_{(0,L)^3} \frac{1}{\Delta t\delta}(\varphi^\delta - \varphi_p)_+\varphi^\delta \ dx - \frac{C\beta}{2\varepsilon}\int_{(0,L)^3} |\mathbf{u}_p|^2(\partial_{\Delta t}\varphi^\delta)_+ \ dx.$$

Using elementary inequalities yields

$$\frac{\varepsilon}{\delta}(\varphi^\delta - \varphi_p)_+\varphi^\delta - \frac{C\beta}{2}|\mathbf{u}_p|^2(\varphi^\delta - \varphi_p)_+ \geq \frac{3\varepsilon}{4\delta}(\varphi^\delta - \varphi_p)_+^2 - \frac{\beta^2 C^2\delta}{4\varepsilon}|\mathbf{u}_p|^4. \tag{56}$$

Putting together estimates (54) and (55), and using inequality (56), yields

$$\begin{aligned} G_c\int_{(0,L)^3} \big(\frac{(\varphi^\delta)^2}{16} + \varepsilon^2|\nabla\varphi^\delta|^2\big) \ dx + \int_{(0,L)^3} \frac{3\varepsilon}{4\Delta t\delta}(\varphi^\delta - \varphi_p)_+^2 \ dx + \\ \frac{\beta C}{2\Delta t}\int_{(0,L)^3} \varphi^\delta|\mathbf{u}^\delta|^2 \ dx + c_1 k||e(\mathbf{u}^\delta)||_{L^2}^2 + \tilde{c}_3||\inf\{\varphi^\delta, 1\}e(\mathbf{u}^\delta)||_{L^2}^2 \leq \\ \tilde{c}_9 + C\int_{(0,L)^3} \frac{\beta^2\delta}{\Delta t\varepsilon}|\mathbf{u}_p|^4 \ dx. \end{aligned} \tag{57}$$

For sufficiently small $\delta \leq C_0\varepsilon$, we obtain from estimates (54) and (57)

$$\frac{\beta}{2\Delta t}\int_{(0,L)^3} \varphi^\delta|\mathbf{u}^\delta|^2 \ dx + c_{10}\varepsilon^2||\nabla\varphi^\delta||_{L^2}^2 + c_3||\tilde{\varphi}^\delta e(\mathbf{u}^\delta)||_{L^2}^2 + ||\varphi^\delta||_{L^2}^2 \leq c_{10}; \tag{58}$$

$$||e(\mathbf{u}^\delta)||_{L^2}^2 \leq \frac{c_{11}}{k} \tag{59}$$

Estimates (58)-(59) imply uniform boundedness of φ^δ in $H^1((0,L)^3)$, with respect to δ. Therefore there exists $\{\mathbf{u}, \varphi\}$ and a subsequence, denoted by the same superscript, such that

$$\begin{gathered} \{\mathbf{u}^\delta, \varphi^\delta\} \to \{\mathbf{u}, \varphi\} \quad \text{weakly in } V_U \times H^1((0,L)^3), \\ \text{strongly in } \ L^q((0,L)^3)^4, \ q < 6, \quad \text{and a.e. on} \quad (0,L)^3, \quad \text{as} \ \ \delta \to +0. \end{gathered} \tag{60}$$

Passing to the limit in equation (46) is straightforward and we conclude that $\{\mathbf{u}, \varphi\}$ satisfies equation (19). As in the proof of Theorem 3, we also conclude

$$\mathbf{u}^\delta \to \mathbf{u} \quad \text{strongly in} \quad V_U, \quad \text{as} \ \ \delta \to +0. \tag{61}$$

In addition

$$(\varphi^\delta - \varphi_p)_+ \to 0, \quad \text{as} \quad \delta \to 0 \quad \text{and} \quad \varphi \in K. \tag{62}$$

Next we use Minty's lemma and write equation (47) in the equivalent form

$$\int_{(0,L)^3} (1-k) \inf\{\varphi^\delta, 1\}(\psi - \varphi^\delta)\mathcal{G}e(\mathbf{u}^\delta) : e(\mathbf{u}^\delta)\ dx + G_c \int_{(0,L)^3} \big(-\frac{1}{\varepsilon}(1-\psi)(\psi - \varphi^\delta)$$
$$+\varepsilon \nabla\psi \cdot \nabla(\psi - \varphi^\delta)\big)\ dx + \int_{(0,L)^3} \frac{1}{\Delta t \delta}(\psi - \varphi_p)_+(\psi - \varphi^\delta)\ dx +$$
$$(1+b)\int_{(0,L)^3} (\inf\{\varphi^\delta, 1\})^b\ (\mathbf{f}\cdot\mathbf{u}^\delta + \mathcal{F} : e(\mathbf{u}^\delta))(\psi - \varphi^\delta)\ dx \geq 0,$$
$$\forall\ \psi \in H^1((0,L)^3) \cap L^\infty((0,L)^3). \tag{63}$$

After taking $\psi \in K$, we pass to the limit $\delta \to 0$ as in classical textbooks (see e. g. [14]) and obtain

$$\int_{(0,L)^3} (1-k)\varphi(\psi - \varphi)\mathcal{G}e(\mathbf{u}) : e(\mathbf{u})\ dx + G_c \int_{(0,L)^3} \big(-\frac{1}{\varepsilon}(1-\psi)(\psi - \varphi) +$$
$$\varepsilon \nabla\psi \cdot \nabla(\psi - \varphi)\big)\ dx + (1+b)\int_{(0,L)^3} \varphi^b\ (\mathbf{f}\cdot\mathbf{u} + \mathcal{F} : e(\mathbf{u}))(\psi - \varphi)\ dx \geq 0,$$
$$\forall\ \psi \in K. \tag{64}$$

Applying once more Minty's lemma, we find out that variational inequality (64) is equivalent to variational inequality (27).
Next we take φ_p as test function in variational inequality (27).

It yields

$$\int_{(0,L)^3} (1-k)\varphi(\varphi - \varphi_p)\mathcal{G}e(\mathbf{u}) : e(\mathbf{u})\ dx +$$
$$\int_{(0,L)^3} \big(-\frac{G_c}{\varepsilon}(1-\varphi_p)(\varphi - \varphi_p) + \frac{G_c}{\varepsilon}(\varphi - \varphi_p)^2 + \varepsilon\nabla\varphi \cdot \nabla(\varphi - \varphi_p)\big)\ dx +$$
$$(1+b)\int_{(0,L)^3} \varphi^b\ (\mathbf{f}\cdot\mathbf{u} + \mathcal{F} : e(\mathbf{u}))(\varphi - \varphi_p)\ dx \leq 0. \tag{65}$$

At this point we recall the elementary inequality

$$2\sqrt{k(1-k)}\varphi \leq (1-k)\varphi^2 + k$$

which, together with estimates (58)-(59), yields

$$||\sqrt{\varphi} e(\mathbf{u})||^2_{L^2} + \int_{(0,L)^3} \varphi\varphi_p \mathcal{G}e(\mathbf{u}) : e(\mathbf{u})\ dx \leq \frac{C}{\sqrt{k}}. \tag{66}$$

Repeating once more the estimates for the phase field equation established before estimate (43) and using estimates (58)-(59) and estimate (66), gives estimate (29). □

Next we prove that we can take the limit $\beta \to 0$.

Since $\varphi \geq 0$, we recall that variational inequality (27) can be written in the simpler equivalent form (67)-(68)

$$\int_{(0,L)^3} (1-k)\varphi\psi \mathcal{G}e(\mathbf{u}) : e(\mathbf{u})\; dx + G_c \int_{(0,L)^3} \big(-\frac{1}{\varepsilon}(1-\varphi)\psi + \varepsilon \nabla\varphi \cdot \nabla\psi \big)\; dx$$
$$+(1+b) \int_{(0,L)^3} \varphi^b (\mathbf{f}\cdot\mathbf{u} + \mathcal{F} : e(\mathbf{u}))\psi\; dx \leq 0,$$
$$\forall\; \psi \in H^1((0,L)^3),\; \psi \geq 0 \;\text{ a.e. on }\; (0,L)^3, \tag{67}$$
$$\int_{(0,L)^3} (1-k)\varphi(\varphi_p - \varphi)\mathcal{G}e(\mathbf{u}) : e(\mathbf{u})\; dx + G_c \int_{(0,L)^3} \big(-\frac{1}{\varepsilon}(1-\varphi)(\varphi_p-\varphi) +$$
$$\varepsilon \nabla\varphi \cdot \nabla(\varphi_p - \varphi) \big)\; dx + (1+b)\int_{(0,L)^3} \varphi^b (\mathbf{f}\cdot\mathbf{u} + \mathcal{F} : e(\mathbf{u}))(\varphi_p - \varphi)\; dx = 0. \tag{68}$$

We observe that equation (68) is the condition of Rice (see e.g. [11]).

Theorem 4. *There exists $\{\mathbf{v},\kappa\} \in V_U \times K$, $\kappa \geq 0$ a.e. in $(0,L)^3$, satisfying variational inequality (67)-(68) and*

$$\int_{(0,L)^3} \big((1-k)\kappa^2 + k\big)\mathcal{G}e(\mathbf{v}) : e(\mathbf{w})\; dx + \int_{(0,L)^3} \kappa^{b+1}(\mathcal{F} : e(\mathbf{w}) +$$
$$\mathbf{f}\cdot\mathbf{w})\; dx = 0,\; \forall\; \mathbf{w} \in V_U. \tag{69}$$

Proof. We start by using $\mathbf{u}^\beta$ as a test function in variational equation (19). We follow the estimates for P_1 in the proof of Proposition 1. Obviously, it is enough to redo the estimates involving β, i.e. estimates (36)-(37)

$$\int_{(0,L)^3} \varphi^\beta \beta \partial_{\Delta t}\mathbf{u}^\beta \cdot \mathbf{u}^\beta\; dx \geq \frac{\beta}{2}\int_{(0,L)^3} \varphi^\beta \partial_{\Delta t}|\mathbf{u}^\beta|^2\; dx = \frac{\beta}{2}\int_{(0,L)^3} \partial_{\Delta t}(\varphi^\beta|\mathbf{u}^\beta|^2)\; dx$$
$$-\frac{\beta}{2}\int_{(0,L)^3} |\mathbf{u}_p^\beta|^2 \partial_{\Delta t}\varphi^\beta\; dx \geq \frac{\beta}{2}\int_{(0,L)^3} \partial_{\Delta t}(\varphi^\beta|\mathbf{u}^\beta|^2)\; dx, \tag{70}$$

$$|\int_{(0,L)^3} (\varphi^\beta)^{1+b}\mathbf{f}\cdot\mathbf{u}^\beta\; dx| \leq \frac{C_{bK}}{\sqrt{k}}\sqrt{k\int_{(0,L)^3} \mathcal{G}e(\mathbf{u}^\beta) : e(\mathbf{u}^\beta)\; dx}. \tag{71}$$

The calculations analogous to the ones from the proof of Proposition 1 yield

$$\frac{\beta}{2h}\int_{(0,L)^3} \varphi^\beta|\mathbf{u}^\beta|^2\; dx + c_3||\varphi^\beta e(\mathbf{u}^\beta)||^2_{L^2} + k||e(\mathbf{u}^\beta)||^2_{L^2} \leq \frac{\tilde{c}_{12}}{k}, \tag{72}$$

with constants independent of β. Getting an H^1-estimate, independent of β, for φ^β, is now straightforward. Passing to the limit $\beta \to 0$ follows the lines of the proof of Theorem 3 . $\square$

4 Numerical approximation

We now formulate finite element approximations to (19) and (27), which are analogues to equations (30)–(31).

For spatial discretization, we apply a standard Galerkin finite element method on quadrilaterals in 2D or hexahedra in 3D. Specifically, we approximate displacements by continuous biquadratics in 2D or trilinears in 3D and refer to the finite element space as V_h. We take φ, $\mathbf{f}$ and $\mathcal{F}$ to be bi- or trilinears in 2D or 3D, respectively, in order to assure continuity, and denote this space as W_h. Here h represents a standard approximation parameter.

In this section, we present the discretization of our phase-field formulation.

$$\int_{(0,L)^3} \big((1-k)(\tilde{\varphi}^h)^2 + k\big)\mathcal{G}e(\mathbf{u}^h) : e(\mathbf{w})\ dx + \int_{(0,L)^3} \beta\varphi_+^h \partial_{\Delta t}\mathbf{u}^h \cdot \mathbf{w}\ dx$$
$$+ \int_{(0,L)^3} (\tilde{\varphi}^h)^{b+1}(\mathcal{F} : e(\mathbf{w}) + \mathbf{f}\cdot\mathbf{w})\ dx = 0 \quad \forall \mathbf{w} \in V_h, \tag{73}$$
$$G_c \int_{(0,L)^3} \big(-\frac{1}{\varepsilon}(1-\varphi^h)\psi + \varepsilon\nabla\varphi^h \cdot \nabla\psi\big)\ dx + \int_{(0,L)^3} \frac{1}{\delta}(\partial_{\Delta t}\varphi^h)_+\psi\ dx +$$
$$(1+b)\int_{(0,L)^3} (\tilde{\varphi}^h)^b(\mathcal{F} : e(\mathbf{u}^h) + \mathbf{f}\cdot\mathbf{u}^h)\psi\ dx +$$
$$\int_{(0,L)^3} (1-k)\tilde{\varphi}^h\psi\mathcal{G}e(\mathbf{u}^h) : e(\mathbf{u}^h)\ dx = 0 \quad \forall\ \psi \in W_h. \tag{74}$$

The incremental formulation (73)-(74) corresponds to the (pseudo-) time stepping scheme based on a difference quotient approximation with backward differences for the time derivatives. In the quasi-static model the time derivatives $\beta\varphi^n\partial_t\mathbf{u}$ and $\frac{1}{\delta}[\partial_t\varphi]_+$ are present. They are discretized as follows

$$\beta\varphi_+\partial_t\mathbf{u} \to \beta\varphi_+\partial_{\Delta t}\mathbf{u} = \beta\varphi_+\frac{\mathbf{u}-\mathbf{u}^{n-1}}{\Delta t}, \quad \frac{1}{\delta}[\partial_t\varphi]_+ \to \frac{1}{\delta}[\partial_{\Delta t}\varphi]_+ = \frac{1}{\delta}\frac{[\varphi-\varphi^{n-1}]_+}{\Delta t},$$

with the time step size Δt, where $n-1$ is used to indicate the preceding time step. We then obtain for the weak form:

$$\beta\varphi_+(\mathbf{u}-\mathbf{u}^{n-1}, \mathbf{w})_{L^2} + \Delta t(A, \mathbf{w})_{L^2} = 0, \quad \forall \mathbf{w} \in V_h, \tag{75}$$
$$\frac{1}{\delta}(\varphi_+ - \varphi_+^{n-1}, \psi)_{L^2} + \Delta t(B, \psi)_{L^2} = 0, \quad \forall \psi \in W_h. \tag{76}$$

Here, $(\cdot,\cdot)$ denotes the discrete scalar product in L^2 and A and B denote the operators of all remaining terms for the present time step in the weak formulation, where equations (75) and (76) are related to equations (73) and (74).

Finally, the spatially discretized semi-linear form can be written in the following way:

Finite Element Formulation 1. *Find* $\mathbf{U}^h := \{\mathbf{u}^h, \varphi^h\} \in V_h \times W_h$ *such that:*

$$A(\mathbf{U}^h)(\mathbf{\Psi}) = \beta\varphi^h_+(\mathbf{u}^h - \mathbf{u}^{h,n-1}, \mathbf{w})_{L^2} + \\ \frac{1}{\delta}([\varphi^h - \varphi^{h,n-1}]_+, \psi)_{L^2} + \Delta t A_S(\mathbf{U}^h)(\mathbf{\Psi}) = 0,$$

with

$$A_S(\mathbf{U}^h)(\mathbf{\Psi}) = \Big(((1-k)(\inf\{\varphi^h_+, 1\})^2 + k)\mathcal{G}e(\mathbf{u}^h), e(\mathbf{w})\Big)_{L^2} - \langle \tau, \mathbf{w}\rangle_{\partial_N\Omega} \\ - ((\inf\{\varphi^h_+, 1\})^{1+b}(\alpha - 1)p_B, \nabla\cdot\mathbf{w})_{L^2} + (\nabla p_B(\inf\{\varphi^h_+, 1\})^{1+b}, \mathbf{w})_{L^2} + \\ \Big((1-k)\mathcal{G}e(\mathbf{u}^h) : e(\mathbf{u}^h)(\inf\{\varphi^h_+, 1\}), \psi\Big)_{L^2} - \frac{G_c}{\epsilon}(1-\varphi^h, \psi)_{L^2} + G_c\epsilon(\nabla\varphi^h, \nabla\psi)_{L^2} \\ - (1+b)\Big((\inf\{\varphi^h_+, 1\})^b(\alpha - 1)p_B\nabla\cdot\mathbf{u}^h, \psi\Big)_{L^2} \\ + (1+b)\Big((\inf\{\varphi^h_+, 1\})^b\nabla p_B\cdot\mathbf{u}^h, \psi\Big)_{L^2} = 0,$$

for all $\mathbf{\Psi} = \{\mathbf{w}, \psi\} \in V_h \times W_h$*, where* $A_S(\cdot)(\cdot)$ *is the sum of equations* (73) *and* (74) *and equality* (16) *is applied in the relation between* τ *and* $\mathcal{T}$*.*

Later in the simulations we choose $b = \frac{1}{2}$.

4.1 Linearization and Newton's method

The nonlinear problem is solved with Newton's method. For the iteration steps $m = 0, 1, 2, \ldots$, it holds:

$$A'(\mathbf{U}^{h,m})(\mathbf{\Delta U}^h, \mathbf{\Psi}) = -A(\mathbf{U}^{h,m})(\mathbf{\Psi}), \quad \mathbf{U}^{h,m+1} = \mathbf{U}^{h,m} + \lambda\mathbf{\Delta U}^h,$$

with $\mathbf{\Delta U}^h = \{\mathbf{\Delta u}^h, \Delta\varphi^h\}$, and a line search parameter $\lambda \in (0, 1]$. Here, we need the (approximated) Jacobian of Finite Element Formulation 1 (defined without using the subscript h):

$$A'(\mathbf{U})(\mathbf{\Delta U}, \mathbf{\Psi}) = \beta\Big(\Delta\varphi_+(\mathbf{u} - \mathbf{u}^{n-1}) + \varphi_+\Delta\mathbf{u}, \mathbf{w}\Big)_{L^2} + \\ \frac{1}{\delta}(\Delta[\varphi - \varphi^{n-1}]_+, \psi)_{L^2} + \Delta t A'_S(\mathbf{U})(\mathbf{\Delta U}, \mathbf{\Psi}),$$

with

$$A'_S(\mathbf{U})(\mathbf{\Delta U}, \mathbf{\Psi}) = \Big(2(1-k)\inf\{\varphi_+, 1\}H(1-\varphi)\Delta\varphi\mathcal{G}e(\mathbf{u}) + ((1-k)(\inf\{\varphi_+, 1\})^2 \\ + k)\mathcal{G}e(\Delta\mathbf{u}), e(\mathbf{w})\Big)_{L^2} - ((1+b)(\inf\{\varphi_+, 1\})^b H(1-\varphi)\Delta\varphi(\alpha - 1)p_B, \nabla\cdot\mathbf{w})_{L^2} +$$

$$((1+b)(\inf\{\varphi_+,1\})^b H(1-\varphi)\Delta\varphi\nabla p_B,\mathbf{w})_{L^2} + \Big(2(1-k)\mathcal{G}e(\mathbf{u}):e(\Delta\mathbf{u})\inf\{\varphi_+,1\}$$
$$+(1-k)\mathcal{G}e(\mathbf{u}):e(\mathbf{u})H(1-\varphi)\Delta\varphi,\psi\Big)_{L^2} + \frac{G_c}{\epsilon}(\Delta\varphi,\psi)_{L^2} + G_c\epsilon(\nabla\Delta\varphi,\nabla\psi)_{L^2} -$$
$$(\alpha-1)(1+b)(p_B(b(\inf\{\varphi_+,1\})^{b-1}H(1-\varphi)\Delta\varphi\nabla\cdot\mathbf{u} + (\inf\{\varphi_+,1\})^b\nabla\cdot\Delta\mathbf{u}),\psi)_{L^2}$$
$$+(1+b)\Big(\nabla p_B\cdot(b(\inf\{\varphi_+,1\})^{b-1}H(1-\varphi)\Delta\varphi\mathbf{u} + (\inf\{\varphi_+,1\})^b\Delta\mathbf{u}),\psi\Big)_{L^2} = 0,$$

for all $\mathbf{\Psi} = \{\mathbf{w},\psi\} \in V_h \times W_h$. $H(\cdot)$ is Heaviside's function.

4.2 Choice of the parameters

It is important to understand the meaning of the various parameters k,β,ϵ,δ and the discretization parameters Δt and h. For the usual parameters in a pure elastic regime, we restate the findings of Bourdin et al. [4]:

- $k \ll 1$ because the elastic moduli are small in the crack and, in addition, should be large enough to stabilize the numerical scheme, but small enough to prevent overestimation of the elastic bulk energy,
- $h < \epsilon \ll 1$ should be small enough to prevent overestimation of the crack surface energy,
- Δt small enough for the crack propagation.

Novel in our work now is the presence of the pressure term p_B so that we have in addition to the previous statements:

- β contributes to the robustness of the algorithm. The theory and computational results demonstrate that the solutions are insensitive with respect to β.
- δ is the penalization parameter which should be chosen appropriately for a given probem.

5 Numerical Tests

We carry out three different tests. In the first example, we neglect the pressure and reproduce benchmark results for crack growth in a pure (brittle) elastic regime [16]. The second test is a modification of Bourdin et al. [6], where a constant pressure $p_B = 10^{-3}$ is injected into the domain. The crack opening displacement and the volume is compared to published values.

The programming code is a modification of the multiphysics program template [23], based on the finite element software `deal.II` (see [2]).

5.1 Single edge notched tension test

In this first example, we compute the single edge notched tension test without using a pressure, i.e., $p_B = 0$. We use this test for code verification for standard examples in pure elasticity. The geometric and material properties are the same as used in [16]. The configuration is displayed in Figure 1. We use $\mu = 80.77kN/mm^2$, $\lambda = 121.15kN/mm^2$, and $G_c = 2.7N/mm$. The crack growth is driven by a non-homogeneous Dirichlet condition for the displacement field on Γ_{top}, the top boundary of Ω . We increase the displacement on Γ_{top} at each time step, namely

$$u_y = \Delta t \times \bar{u}, \quad \bar{u} = 1 \text{ mm}.$$

Furthermore, we set $k = 2.2 \times 10^{-2}, \epsilon = 4.4 \times 10^{-2}$ mm and the mesh size parameter is chosen as $h \sim 2.2 \times 10^{-2} mm$. Computations are shown for three different time steps $\Delta t = 10^{-4}s, 5 \times 10^{-5}s$ and $10^{-5}s$.

We also run tests on a locally refined mesh with minimal $h = 2.76 \times 10^{-3}$ mm and as shown in Figure 1. The parameters δ and β are not important for this elasticity example and we choose $\delta = \infty$ and $\beta = 10^{-8}\ kN/mm^4$.

We evaluate the surface load vector on the Γ_{top} as

$$\tau = (F_x, F_y),$$

where we are particularly interested in F_y as illustrated in Figure 2, we identify the same behavior for the load-displacement curve as observed in [16].

In Figure 3, we identify the crack pattern for three different displacement steps. The locally pre-refined mesh is displayed in Figure 1. Finally, Figure 4, shows the sharp jump in the displacement in the y direction. Later, the jump can be used to determine the width of the fracture.

From our numerical observations, the most critical choice for a fixed $\epsilon := 2h$ in this setting is the parameter k, which strongly determines when the crack starts to grow. This agrees with the theory and the parameter relations outlined in Section 4.2.

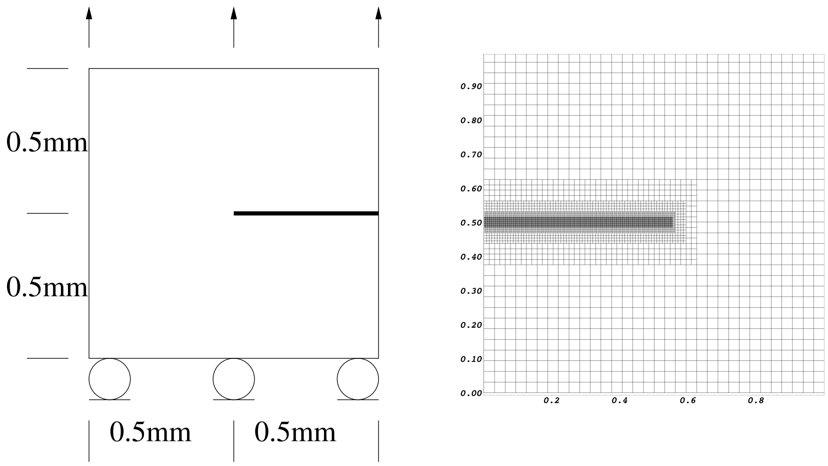

Figure 1: Example 1: Single edge notched tension test: configuration (left) and mesh.

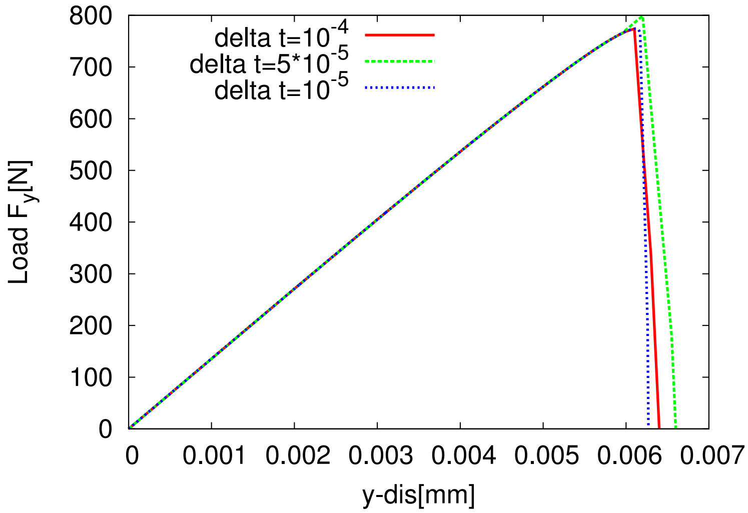

Figure 2: Example 1: Single edge notched tension test: load-displacement curves for different time steps.

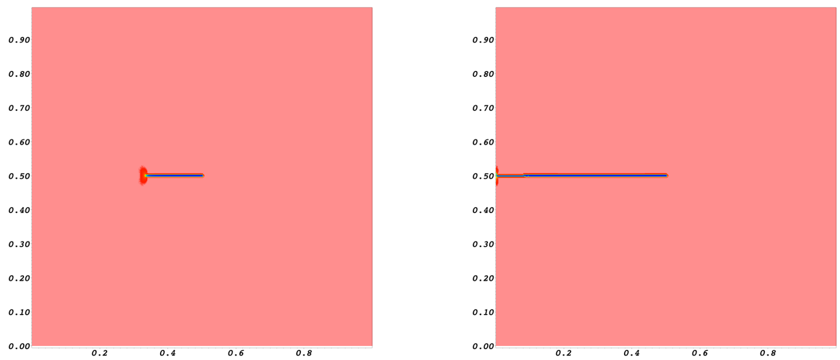

Figure 3: Example 1: Single edge notched tension test: crack pattern for two different displacement steps.

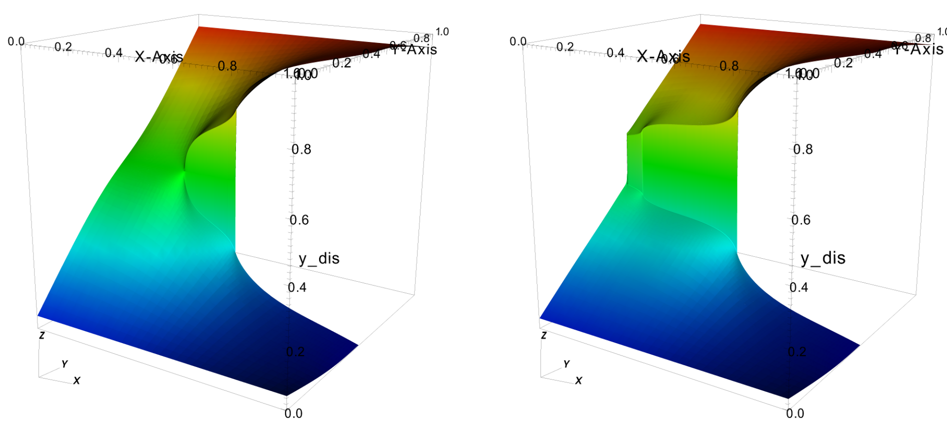

Figure 4: Example 1: Single edge notched tension test: surface plot of the y-displacement. We identify the sharp front in the jump of the normal displacement.

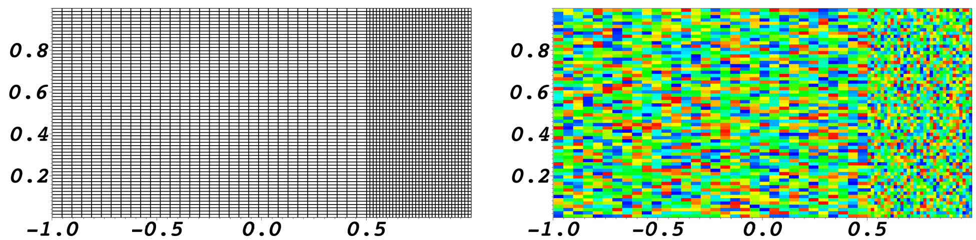

Figure 5: Example 1 with hetereogeneous material: Mesh and μ-distribution.

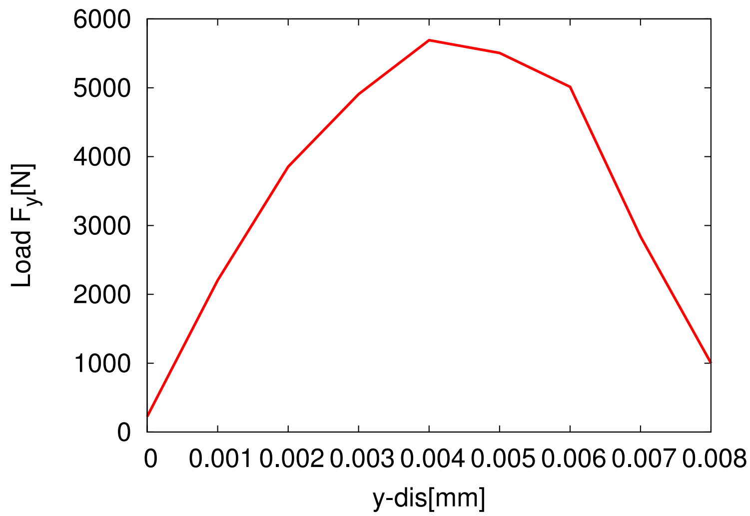

Figure 6: Example 1 with hetereogeneous material: Single edge notched tension test: load-displacement curve.

We extend the previous configuration in order to demonstrate the performance of approach. The distributed Lamé coefficients are used to simulate a heterogeneous material. This leads to non-planar crack-growths, branching and joining of cracks without any modifications in the program. The Lamé parameters are randomly distributed. The previous configuration is modified with respect to the geometry and the μ-λ-fields as displayed in Figure 5. Here, μ varies between $8.1 \times 10^4 - 5.8 \times 10^5$ and λ varies between $1.2 \times 10^5 - 6.2 \times 10^5$. All the other parameters remain the same as in the previous test. The load-displacement curve is observed in Figure 6. Finally, the crack path in this setting is shown in Figure 7.

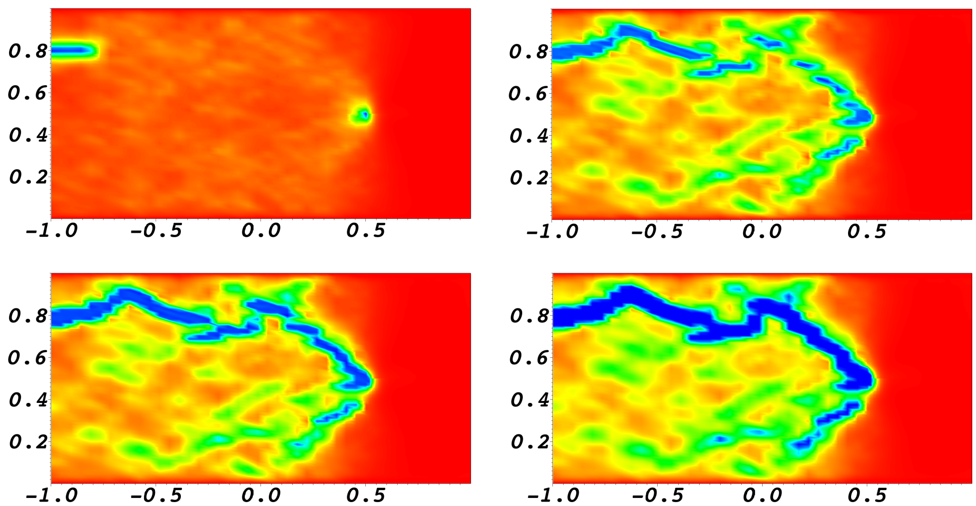

Figure 7: Example 1 with hetereogeneous material: Crack path for different time steps.

5.2 Constant pressure in a crack

The second example is motivated by Bourdin et al. [6] and is based on Sneddon's theoretical calculations [21, 20]. Specifically, we consider a 2D problem where a (constant) pressure p_B is used to drive the deformation and crack propagation. We assume a dimensionless form of the equations.

The configuration is displayed in Figure 8. We prescribe the initial crack implicitly (see e.g. Borden et al. [3]). Therefore, we deal with the following geometric data: $\Omega = (0,4)^2$ and a (prescribed) initial crack on the $y = 4.0$-line $\Omega_C = (1.8, 2.2) \subset \Omega$ with length $2l_0 = 0.4$. As boundary conditions we set the displacements zero on $\partial\Omega$. We perform 5 time steps with time step size $\Delta t = 1.0$.

We fix in the following all computations the regularization parameters $\epsilon = 2.2 \times 10^{-2}$ and $k = 1.1 \times 10^{-3}$. For studies in which they vary, we refer the reader to [6]. The Biot coefficient is $\alpha = 0$. The fracture toughness is chosen as $G_c = 1.0$. The mechanical parameters are Young's modulus and Poisson's ration $E = 1.0$ and $\nu_s = 0.2$. The injected pressure is $p_B = 10^{-3}$.

Several tests are performed:

- Spatial mesh convergence:
  Fix $\epsilon, k, \delta = 10^{-5}, \beta = 1$:
  Vary $h = 2.2 \times 10^{-2}, 1.1 \times 10^{-2}, 5.5 \times 10^{-3}$,
- Ratio ϵ to h is fixed:

Fix $k, \delta = 10^{-5}, \beta = 1$:
Vary $\epsilon = h = 2.2 \times 10^{-2}, 1.1 \times 10^{-2}, 5.5 \times 10^{-3}$,

- Influence of the penalization parameter δ:
  Fix $\epsilon, k, \beta = 1, h = 1.1 \times 10^{-2}$:
  Vary $\delta = 10^{-3}, 10^{-4}, 10^{-5}$,

- Influence of the friction stabilization parameter β:
  Fix $\epsilon, k, \delta = 10^{-5}, h = 1.1 \times 10^{-2}$:
  Vary $\beta = 10^{0}, 10^{-8}$.

The goal is to measure the crack opening displacement and the volume of the crack. To do so, we observe u along Ω_C. Specifically, the width is determined as the jump of the normal displacements:

$$w = COD = [\mathbf{u} \cdot \mathbf{n}]. \tag{77}$$

Expression (77) can be written as

$$w = COD = \int_{\infty}^{\infty} \mathbf{u} \cdot \nabla\varphi \, dy,$$

where φ is as before our phase-field function. Second, following [9], p. 710, the volume of the fracture is:

$$V = \pi w l_0$$

The analytical expression for the width (to which we compare) [9] is:

$$w = 4\frac{(1 - \nu_s^2) l_0 p}{E},$$

Then, the analytical expression for the volume becomes

$$V = 2\pi \frac{(1 - \nu_s^2) l_0^2 p}{E}. \tag{78}$$

In contrast to [6], we use the numerical approximation of the phase-field function instead of a synthetic choice of the crack indicator function.

The crack pattern and the corresponding mesh are displayed in Figure 8. In Figures 9-12, the solutions for different set of parameters are displayed. We observe that the choice of δ has most influence on the final crack opening displacement as seen at Figure 11. This is a well known difficulty from the numerical approximation of variational inequalities (see e.g. [12]). Our findings for different spatial mesh parameters h show different results (see Figure 9). Finally, (as already shown in the theoretical part of this work), the friction parameter β does not influence the final result. In fact, for different β all three graphs in Figure 12 coincide.

The obtained crack volumes are displayed in Table 2 in which the exact value is computed by Formula (78).

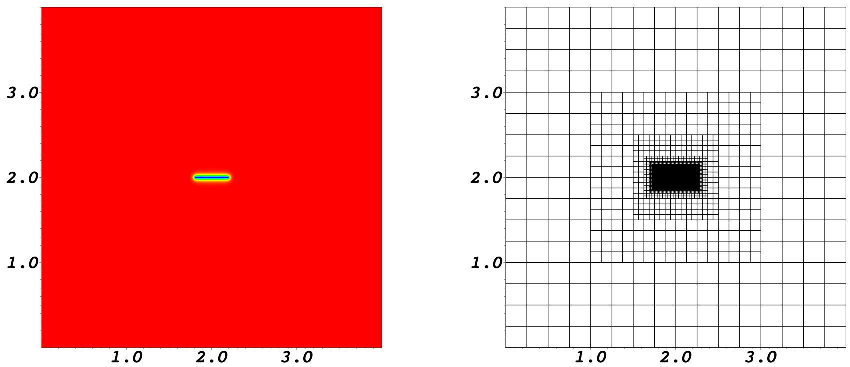

Figure 8: Example 2: Configuration (left) and final crack pattern (right).

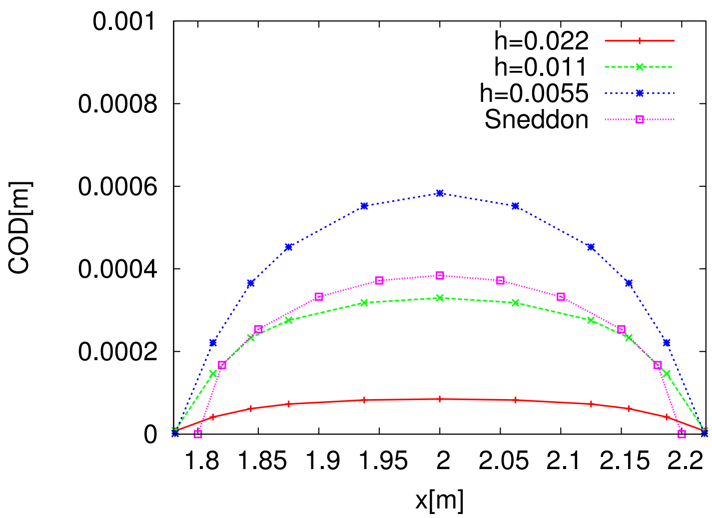

Figure 9: Example 2: COD for different h. Sneddon's pink line with squares corresponds to his analytical solution.

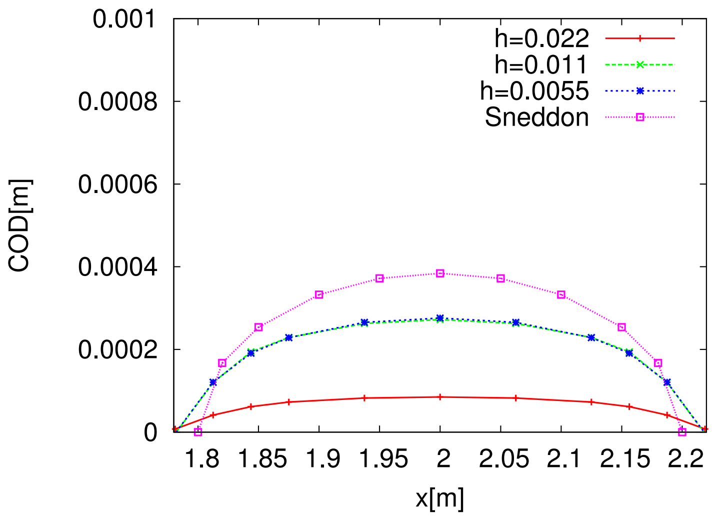

Figure 10: Example 2: COD for different ϵ. Sneddon's pink line with squares corresponds to his analytical solution.

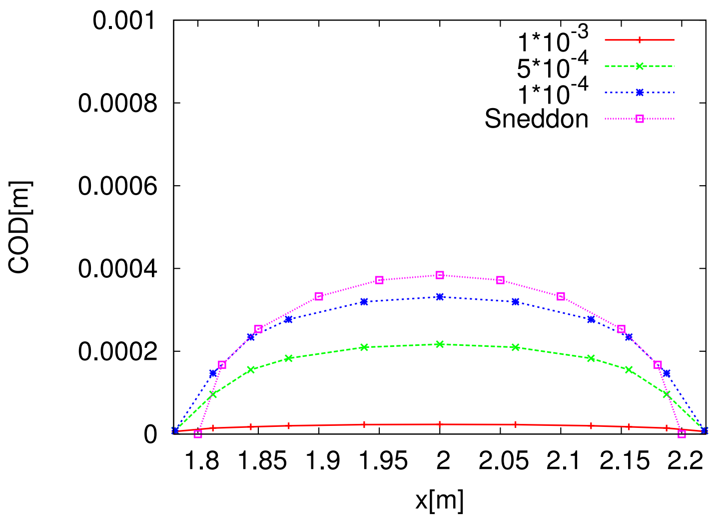

Figure 11: Example 2: COD for different δ. Sneddon's pink line with squares corresponds to his analytical solution.

Table 2: Example 2: Volume in the fracture for different h, δ and β, respectively.

h	2.2×10^{-2}	1.1×10^{-2}	5.5×10^{-3}	exact
V	5.34×10^{-5}	2.07×10^{-4}	4.00×10^{-4}	2.41×10^{-4}
δ	10^{-3}	5×10^{-4}	10^{-5}	
V	1.47×10^{-5}	1.36×10^{-4}	2.08×10^{-4}	2.41×10^{-4}
β	10^{0}	10^{-4}	10^{-8}	
V	2.08×10^{-4}	2.07×10^{-4}	2.07×10^{-4}	2.41×10^{-4}

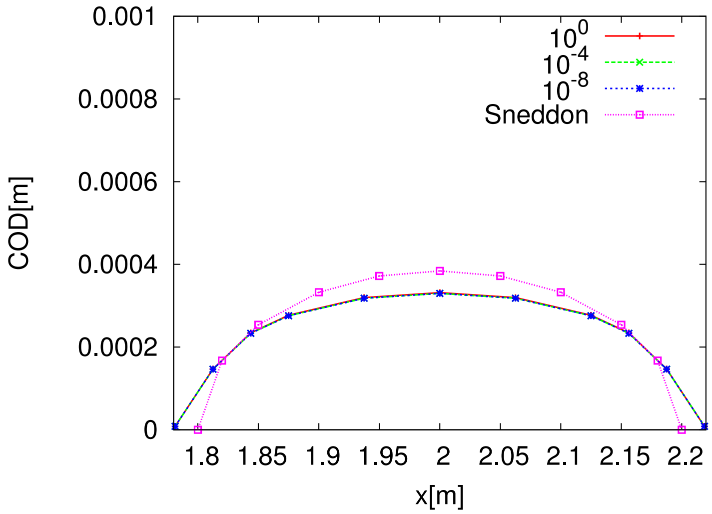

Figure 12: Example 2: COD for different β. Sneddon's pink line with squares corresponds to his analytical solution.

5.3 Nonconstant pressure in the crack

We extend the previous example by applying the pressure equation (2) to inject a fluid in the crack. The following parameters are used: $k = 1.1 \times 10^{-3}, \epsilon = 4.4 \times 10^{-2}, \beta = 1.0, G_c = 1.0 \times 10^{7}, \delta = 10^{-12}, \nu_s = 0.2, E = 10^{9}$.

The parameters of the pressure equations are $M = 2.5 \times 10^{8}, \alpha = 0, \mu = 1.0$. In particular, the permeability is higher for the fracture cells, i.e., $K = 10^{-13}$ in the reservoir and in the fracture $K = 10^{-12}$.

In each time step we inject fluid with a constant rate of $q_I = 1.0e - 5$. In Figure 13, we observe an increasing pressure until the crack starts growing and the pressure decreases. This is a well-known effect in hydraulic fracturing.

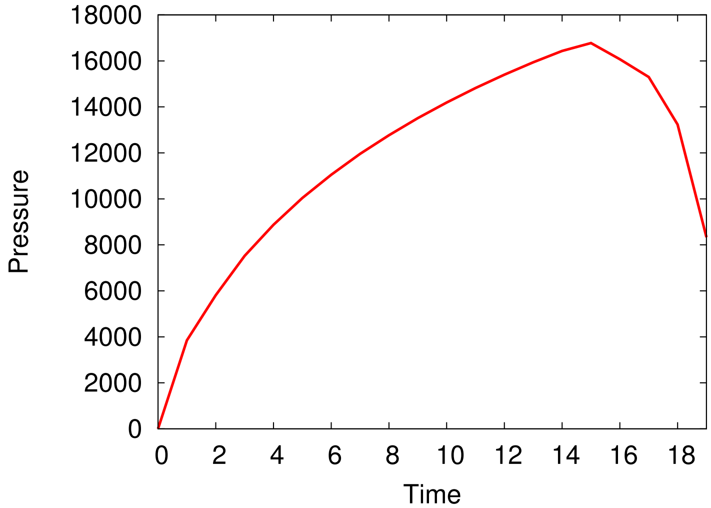

Figure 13: Example 2 with constant flow injection at a constant rate: Pressure versus time.

5.4 3D test: Penny-shape crack growth

This example has three important features:

- Extension to three dimensions with an initially prescribed penny-shape crack,
- A (single-phase) fluid is injected into the crack,
- Pressure is non-constant and computed fom the pressure equation (2).

We consider the unit cube and prescribe a given crack in the $y = 0.5$-plane with radius 0.1 as displayed in Figure 14. Moreover, to reduce the computational cost, local mesh refinement as shown in Figure 15 is used. At all boundaries the homogeneous Dirichlet conditions for the displacement are imposed, except at the top boundary, which is traction free. The material parameters are similar to [6] (see page 5); that is $\mu = 1$ and $\nu_s = 0.3$. The fracture toughness is $G_c = 1.91 * 10^{-9}$. Then, $k = 0.11, \epsilon = 0.22, \beta = 1.0$. The time step is chosen as $\Delta t = 1.0$. The injection rate is $q_I = 5.0 \times 10^{-10}$.

We prescribe an injection in the middle of the domain as illustrated in Figure 16. The pressure parameters are $M = 2.5 \times 10^8, \alpha = 0, \eta = 1.0, K = 10^{-13}, \rho_f = 1.0$. The initial pressure is $p_{in} = 10^{-2}$.

As observed in the previous section the friction parameter does not play a significant role. Therefore, we perform six tests, i.e., for three different h (leading to $960, 1408, 5888$ cells and indicated with 'Level 1,2,3' below) and two different $\delta = 10^{-2}$ and 10^{-4}.

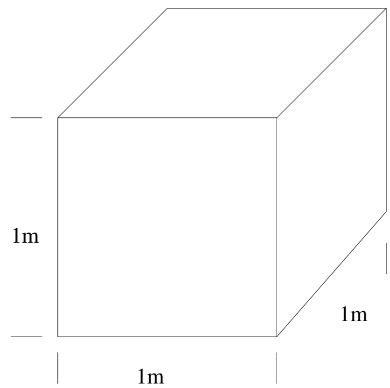

Figure 14: Example 3: Configuration.

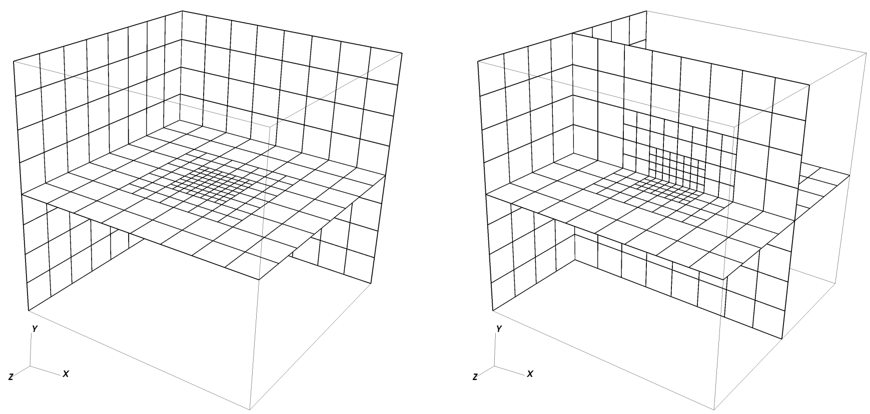

Figure 15: Example 3: Locally refined meshes.

We observe the following behaviors:

- Time evolution of u_y at $(0.5, 0.5, 0.5)$,
- Time evolution of u_y at $(0.5, 1.0, 0.5)$,
- Time evolution of pressure in $(0.5, 0.5, 0.5)$,
- End-time u_y values in x-direction in the $y = 0.5$-plane at fixed $z = 0.5$.

We see in the results in Figure 19-21 a relative strong influence of the mesh size h, which indicates a need for a sufficiently refined meshes.

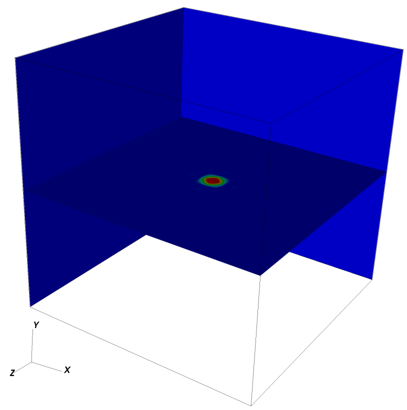

Figure 16: Example 3: Pressure field. The highest pressure (at the injection well) is indicated in red in the middle of the domain.

6 Conclusion

In this paper we have presented a (b, β)-family of phase field algorithms for modeling a fluid filled fracture in a poroelastic medium based on an incremental formulation. Existence of a weak solution to the incremental phase field problem is established through a priori estimates. Several benchmark numerical results are demonstrated. This approach can treat heterogeneous porous media and allows for crack branching. Ongoing computations involve coupling this framework to a multiphase reservoir simulator for modeling hydraulic fracturing as well as treating intersecting fractures.

References

[1] J. Adachi, E. Siebrits, A.Peirce, J. Desroches, Computer simulation of hydraulic fractures, International Journal of Rock Mechanics and Mining Sciences, Vol. 44 (2007), p. 739–757.

[2] W. Bangerth, T. Heister, G. Kanschat, Differential Equations Analysis Library, 2012.

[3] M. J. Borden, C. V. Verhoosel, M. A Scott, T. J. R. Hughes, C. M. Landis, A phase-field description of dynamic brittle fracture, Computer Methods in Applied Mechanics and Engineering, Vol. 217 (2012), p. 77-95.

[4] B. Bourdin, G.A. Francfort, J.-J. Marigo, Numerical experiments in revisited brittle fracture, J. Mech. Phys. Solids, 48 (4) (2000): 797–826.

[5] B. Bourdin, G.A. Francfort, J.-J. Marigo, The Variational Approach to Fracture, J. Elasticity 91 (1-3) (2008): 1–148.

[6] B. Bourdin, C. Chukwudozie, K. Yoshioka, A Variational Approach to the Numerical Simulation of Hydraulic Fracturing, SPE Journal, Conference Paper 159154-MS, 2013, doi 0.2118/159154-MS.

[7] R. de Borst, J. Rethoré, M.A. Abellan, A numerical approach for arbitrary cracks in a fluid-saturated porous medium, Arch. Appl. Mech. 75 (2006) 595–606.

[8] R. Calhoun, M. Lowengrub, A two dimensional asymmetrical crack problem, J. Elasticity, Vol. 4 (1974), p. 37-50.

[9] R.H. Dean, J.H. Schmidt, Hydraulic-Fracture Predictions with a fully coupled geomechanical reservoir simulator, SPE Journal, (2009), p. 707-714.

[10] G.A. Francfort, J.-J. Marigo, Revisiting brittle fracture as an energy minimization problem. J. Mech. Phys. Solids. 46 (8) (1998) : 1319–1342.

[11] G.A. Francfort, Un résumé de la théorie variationnelle de la rupture, Séminaire Laurent Schwartz – EDP et applications, Institut des hautes études scientifiques, 2011-2012, Exposé no. XXII, 1-11. `http://slsedp.cedram.org/slsedp-bin/fitem?id=SLSEDP_2011-2012`

[12] Glowinski, R., Lions, J. L., Trémolières, R. (1976). Analyse numérique des inéquations variationnelles. Dunod.

[13] F. Irzal, J. J.C. Remmers, J. M. Huyghe, R. de Borst, A large deformation formulation for fluid flow in a progressively fracturing porous material, Comput. Methods Appl. Mech. Engrg. Vol. 256 (2013), p. 29–37.

[14] D. Kinderlehrer, G. Stampacchia, An introduction to variational inequalities and their applications. Reprint of the 1980 original. Classics in Applied Mathematics, 31. Society for Industrial and Applied Mathematics (SIAM), Philadelphia, PA, 2000. xx+313 pp.

[15] C. Miehe, F. Welschinger, M. Hofacker, Thermodynamically consistent phase-field models of fracture: variational principles and multi-field FE implementations, International Journal of Numerical Methods in Engineering, 83 (2010):1273–1311.

[16] C. Miehe, M. Hofacker, F. Welschinger, A phase field model for rate-independent crack propagation, Comput. Meth. Appl. Mech. Engrg., 199 (2010):2765–2778.

[17] A. Mikelić, M. F. Wheeler: Convergence of iterative coupling for coupled flow and geomechanics, Comput Geosci, Vol. 17 (2013), no. 3, p. 455-462. DOI 10.1007/s10596-012-9318-y.

[18] A. Mikelić , B. Wang, M. F. Wheeler, Numerical convergence study of iterative coupling for coupled flow and geomechanics, submitted, March 2013.

[19] S. Secchi and B. A. Schrefler, A method for 3-D hydraulic fracturing simulation, Int J Fract , Vol. 178 (2012), p. 245–258.

[20] I. N. Sneddon, The distribution of stress in the neighbourhood of a crack in an elastic solid, Proc. R Soc London A, Vol. 187 (1946), p. 229-60.

[21] I. N. Sneddon, M. Lowengrub, Crack problems in the classical theory of elasticity. The SIAM series in Applied Mathematics. John Wiley and Sons (1969).

[22] I. Tolstoy, ed., Acoustics, elasticity, and thermodynamics of porous media. Twenty-one papers by M.A. Biot, Acoustical Society of America, New York, 1992.

[23] T. Wick, Solving monolithic fluid-structure interaction problems in arbitrary Lagrangian Eulerian coordinates with the deal.ii library, 2013. Archive for Numerical Software, Vol. 1, pp. 1-19, www.archnumsoft.org/

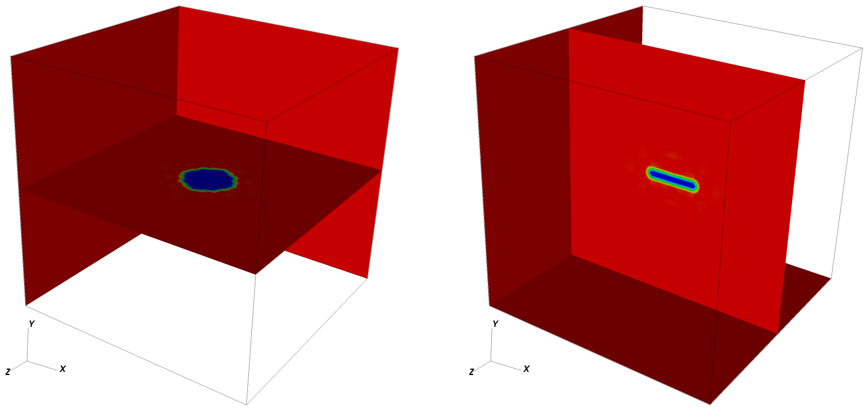

Figure 17: Example 3: Phase-field function at the end time step in the $y = 0.5$-plane. The blue-region displays the penny-shape fracture.

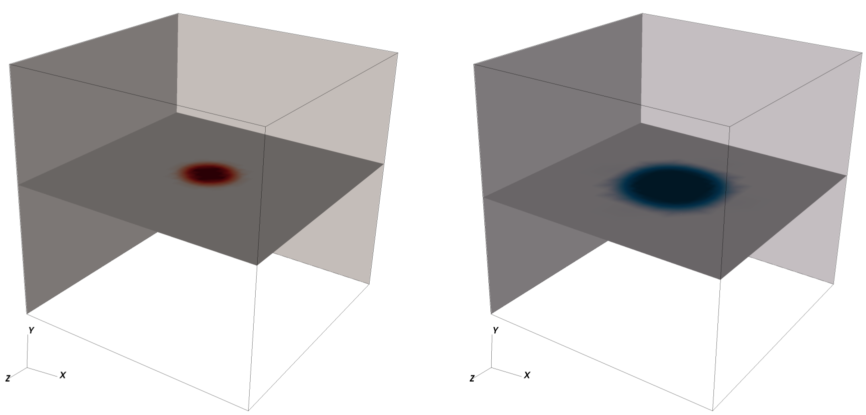

Figure 18: Example 3: y-displacements in the y-direction (normal direction to the fracture at left. In the middle and right, the y-displacement on top $y = 0.55$ and below $y = 0.45$ the fracture are displayed. Red indicates uplift displacement and blue downward displacement.

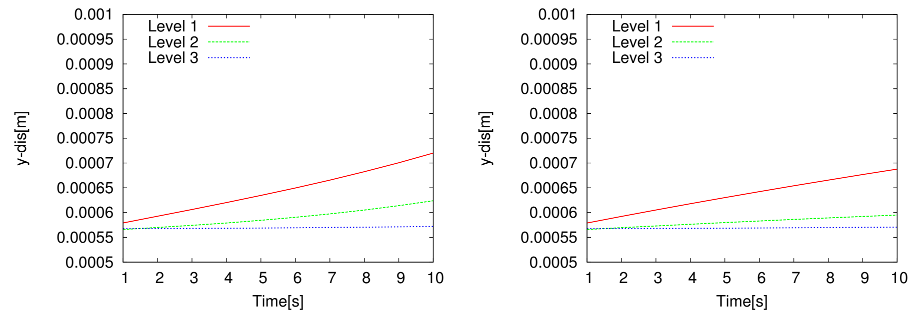

Figure 19: Example 3: Time evolution of the y-displacements in the point $(0.5, 0.5, 0.5)$ for $\delta = 10^{-2}$ (left) and $\delta = 10^{-4}$ (right).

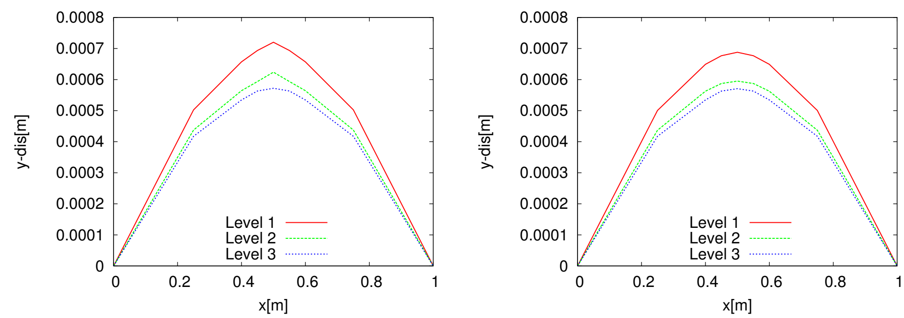

Figure 20: Example 3: y-displacements in x-direction in the $y = 0.5$-plane for fixed $z = 0.5$ for $\delta = 10^{-2}$ (left) and $\delta = 10^{-4}$ (right).

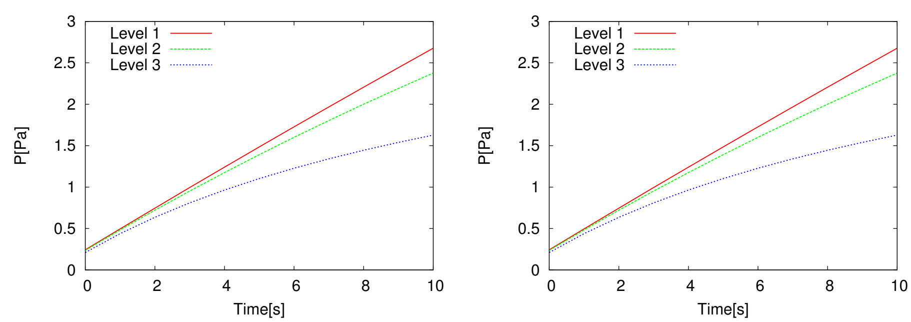

Figure 21: Example 3: Time evolution of the Biot pressure in the point $(0.5, 0.5, 0.5)$ for $\delta = 10^{-2}$ (left) and $\delta = 10^{-4}$ (right).